KTH ROYAL INSTITUTE
OF TECHNOLOGY

Degree Project in the Field of Technology Vehicle Engineering and the Main Field of Study Mathematics

Second cycle, 30 credits

Adjoint-based Formulation for Shape Optimization Problems in Computational Fluid Dynamics

ANTON SCOTTE

Stockholm, Sweden, 2023

Adjoint-based Formulation for Shape Optimization Problems in Computational Fluid Dynamics

ANTON SCOTTE

Master's Programme, Applied and Computational Mathematics, 120 credits
Date: December 14, 2023

Supervisor: Pritpal Matharu
Examiner: Mattias Sandberg
School of Engineering Sciences
Swedish title: Adjointbaserad metod för optimering av geometrier med strömningsmekaniska beräkningar

Abstract

A continuous adjoint formulation for exterior optimization of Dirichlet data on the boundary for potential flow applications has been developed in this thesis. This has been performed by utilizing boundary integral methods for both the primal problem (Laplace's equation) and for the corresponding adjoint equation (Poisson's equation) on the unit disc. A considerable portion is devoted to the estimation of the boundary flux for Poisson's equation. The boundary flux is the (unique) Riesz-representer that determines the search direction in descent methods where the optimal control problem is to reconstruct the Dirichlet data on the boundary in order to minimize a quadratic functional.

Sammanfattning

I denna uppsats behandlas adjoint baserad optimering av Dirichlet data på randen för exteriöra problem relaterat till fluiddynamik. Detta har gjorts med randintegral-metoder för det primära problemet (Laplace's ekvation) samt för den korresponderande adjoint-ekvationen (Poisson's ekvation). Ett stort fokus är estimering av flödet vid randen för Poisson's ekvation på enhetsdisken. För det primära Dirichlet problemet så bestämmer detta flöde sökriktningen i gradientbaserade optimeringmetoder där målet är att rekonstruera Dirichlet-datat på randen för att minimera en kvadratisk funktional.

Dedication

Dedicated to Axel Mark. 1917-2008.

Acknowledgment

I would like to express my gratitude to Pip for taking time out of his schedule to support me whilst working on the thesis and for introducing me to the interesting areas of Adjoint calculus and Boundary Element Methods. We have had many fruitful discussions throughout this year and he has taught me a lot. Thank you Pip.

Stockholm, December 2023

Anton Scotte

Contents

List of Acronyms

BIE Boundary Integral Equation/s

BEM Boundary Element Method

BEMs Boundary Element Methods

IBEM Indirect Boundary Element Method

DBEM Direct Boundary Element Method

FEM Finite Element Method

PDE Partial Differential Equation

FMM Fast Multipole Method

FDM Finite Difference Method

FVM Finite Volume Method

GMRES Generalized Minimal Residual Method

NACA National Advisory Committee for Aeronautics

NSE Navier-Stokes Equations

List of Figures

List of Tables

Chapter 1

Introduction

Engineering problems in aerodynamics often gives rise to large scale optimization problems. Exterior shape optimization problems such as reducing drag or increasing lift-to-drag ratio for an airfoil are examples of such problems. Here we consider Partial Differential Equation (PDE)-constrained optimization. Obtaining efficiency and accuracy when approximating the PDE is crucial. Utilizing numerical methods that have spectral accuracy is sought after, where convergence to the true solution is exponential. Boundary Element Methods (BEMs) are numerical methods that have the advantage of demonstrating spectral accuracy. Moreover, as will be shown, another key advantage of BEMs is that it is often possible to avoid interior domain discretization. For the optimization problems and associated algorithms presented in this thesis, adjoint calculus will be utilized. As will be shown, adjoint calculus can be employed to formulate the expressions for the gradient direction as well as the momentum term in non-linear conjugate gradient methods. In particular, this thesis has its focus on exploring how well adjoint calculus can be utilized in combination with BEMs. The motivation for this work is to develop these methods for exterior aerodynamic/fluid mechanics applications such as the flow around an airfoil with the hope of developing an adjoint-based optimization Boundary Element Method (BEM) solver for the Navier-Stokes Equations (NSE). Indeed, developing a BEM solver for the NSE (without any shape optimization) is a very ambitious project on its own. This thesis instead only focus on the Laplace & Poisson equations, to be used as a stepping stone to dealing with the larger problem of the NSE. The end result of this thesis consist of a prototype for shape optimization where Dirichlet data is reconstructed on the boundary of the unit disc.

1.1 Outline of Shape Optimization Problem

For an incompressible, inviscid and irrotational fluid, the flow can be described with potential theory and the velocity potential of the flow is described by Laplace's equation $\Delta\rho = 0$ [10]. This model does not take into account viscous forces, thus the potential flow description of the flow around an airfoil is only valid outside of the boundary layer. Even though it is important to consider the viscous forces that occur inside the boundary layer, the potential flow model is still an important tool for design of airfoils. In the early days of airfoil design, the Joukowski airfoil was used. The shape of a Jouwkoski airfoil is obtained via a Jouwkowski transform, which is a conformal mapping to the circle [20]. The Joukowski transform is

$$z = \zeta + \frac{1}{\zeta},$$

where $\zeta = \xi + i\eta$ and $z = x + iy$ are complex variables [20]. The airfoil is obtained in the z-plane by applying the Joukowski transform to a circle in the ζ-plane. By changing the center coordinate of the circle, the shape in the z-plane is modified. The Joukowski airfoil lends itself well for describing the solution to the potential flow around the airfoil and for these airfoils it is possible to find analytic solutions. In these days however, they are more used as basic examples in introductory aerodynamic courses. However, this airfoil can provide important insights into many aspects of potential theory, and for this reason it is briefly mentioned here. In the 1920s and 1930s, the National Advisory Committee for Aeronautics (NACA) family of airfoils was developed. A NACA airfoil is developed using a standardized series of digits that specify critical geometric features such as for example, camber lines or maximum thickness for the airfoil [17]. As an example, for a 4-digit NACA airfoil, the first digit specifies the camber as a fraction of the coord length, the second digit specifies the distance from the leading edge as a fraction of the coord length and the last two digits specify the thickness as a fraction of the coord length [17]. If one seeks to alter the shape of either the Joukowski airfoil or the NACA airfoil one is faced with the limitation that the change is parameter-based. For instance, for a NACA-type airfoil, in an optimization setting, one design parameter is altered and a simulation is performed to approximate an output quantity such as drag force. The result from the simulation is used to optimize for the output quantity with respect to this parameter. This procedure has to be performed for each design parameter and it quickly becomes a problem since computational resources are limited. It would be beneficial to be able to perturb the geometry of the airfoil without being limited to optimizing for one design parameter only. This is the point of entry in this thesis work. Conceptually, the idea is to start with an initial geometry such as a circle, and to consider a perturbation vector θ such that the shape is reconstructed to optimize for a quantity such as lift-to-drag ratio.

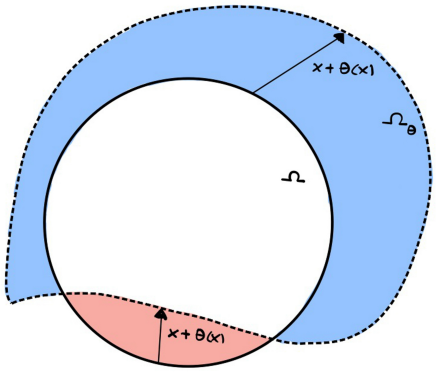

Figure 1.1: Conceptual drawing of a geometric shape optimization problem.

In Figure (1.1), some area is removed (red) and some area is added (blue) to the disc. This change is determined by the perturbation $\theta(x)$ at a given point x on the boundary.

1.2 Structure of thesis

Chapter (2) is devoted to deriving an adjoint optimization framework based on the non-linear conjugate gradient method Polak-Ribiere. Here, adjoint calculus is utilized to determine the conjugate direction and momentum term needed for the Polak-Ribiere method. The PDE we are interested in is Laplace's equation subject to Dirichlet boundary data. In this section it will become clear that the boundary flux when considering a homogenous Poisson problem (the Adjoint system) is a key quantity. Chapter (3) is devoted to BEMs for Laplace's equation. Chapter (4) deals extensively with Poisson solvers for the boundary flux for the interior Dirichlet problem on the disc. In Chapter (5) a prototype for shape optimization is discussed, here the adjoint optimization framework is revisited where the Dirichlet data is reconstructed on the unit disc utilizing the boundary flux information obtained from solving the Poisson problem. Finally in Chapter (6) further research suggestions are presented and the relevance of the model problem developed in this thesis is put into context for future development in the field.

Chapter 2

Optimal Control and Adjoint Calculus

This chapter is devoted to introducing the mathematical tools for adjoint optimization which is revisited in Chapter (5) utilizing the BEM solvers discussed in Chapter (3).

2.1 Optimal Control

We consider a continuous optimal control parameter $\phi \in L^2(\Omega)$ in a PDE where $u(\phi)$ is a solution to the PDE, this creates a PDE-constrained optimization problem. Given a scalar valued objective functional $\mathcal{J}(u(\phi))$ as a quantity of interest, where $\mathcal{J}(u(\phi))$ is here considered as an L^2 inner product on Ω, an optimal control variable $\widehat{\phi} = \arg\min_{\phi \in L^2(\Omega)} \mathcal{J}(u(\phi))$ that minimize the functional is to be determined. In this thesis, the PDE constraint is Laplace's equation defined on a domain Ω, subject to Dirichlet boundary conditions on the boundary Γ. In particular, the sensitivity $\nabla_\phi \mathcal{J}$ with respect to some perturbation vector ϕ' in the boundary data determine the effect a perturbation of the optimal control variable has on the system [18]. Given an initial guess for the control, $\phi^{(0)} = \phi_{initial}$ the optimal control variable satisfies

$$\lim_{n \to \infty} \phi^{(n+1)} \to \widehat{\phi}, \tag{2.1}$$

where some gradient-based descent method is employed to determine $\widehat{\phi}$ for some $\nabla_\phi \mathcal{J}$ at iteration n for $\phi^{(n)}$

$$\phi^{(n+1)} = \phi^{(n)} - \tau \nabla_\phi \mathcal{J}(\phi^{(n)}), \tag{2.2a}$$

$$\phi^{(0)} = \phi_{initial}, \tag{2.2b}$$

and τ is the step length at iteration n. Gradient-based optimization schemes do not guarantee finding a global

minimum, local minima can be found away from a global minimum. The convex quadratic functional

$$\mathcal{J}(u(\phi)) = \frac{1}{2}\int_{\Omega}\left[u(\phi) - u_{target}\right]^2 dx, \tag{2.3}$$

is considered, it is clear that the functional has a global minimum when $u(\phi) = u_{target}$. In (2.3), $u_{target} := u(\widehat{\phi})$ is a known target state and $u(\phi)$ is the state to be determined for a manufactured toy-problem. If not otherwise stated, the following test function for the optimal control variable $\widehat{\phi}$ is used

$$\widehat{\phi} = \Im\left\{\frac{z^2}{z - z_p}\right\}, \tag{2.4}$$

where $\Im\{\}$ denotes the imaginary part, z, $z_p \in \mathbb{C}$, $z \in \Gamma$ and $z_p \notin \Omega$ [1]. The point z_p is chosen as an exterior point to the domain

$$z_p = R_{ext}e^{i\theta}, \tag{2.5}$$

where R_{ext} is chosen such that $z_p \notin \Omega \; \forall \; \theta \in [0, 2\pi]$.

2.2 Polak-Ribiere (Non-linear Conjugate Gradient)

The convergence of the steepest descent method (2.2a) degrades as the system becomes ill-conditioned [24]. Conjugate gradient methods improve convergence rates [24]. In this work the non-linear conjugate gradient method, the Polak-Ribiere method, is employed. For quadratic functions, the Polak-Ribiere method coincides with the linear conjugate gradient method [32]. The Polak-Ribiere method is considered as the intention for this optimization framework is to build towards non-linear problems such as the NSE. Typically in literature, conjugate gradient methods are introduced for discrete systems of equations (e.g. [24]). For a finite dimensional optimization problem, this requires a priori information of the underlying discretization method. Arguably, the most common approach in adjoint based optimization for fluid dynamics is by considering a "discretize-then-optimize" approach. Several researchers have taken such an approach which first leads to a discrete system of equations to be optimized with some gradient-based descent method [23],[15], [16], [18]. In this thesis work, an "optimize-then-discretize" approach [28], [18], [34] is employed rather than the "discretize-then-optimize" approach. As will be shown, this allows the formulation of the optimization problem to be general and independent on the choice of discretization method, the term *continuous formulation* is here used to refer to this and in the following sections the term *continuous adjoint formulation* is used in the same sense.

[1] The reason for working in complex variables will become clear in Section (3.2) on Boundary Integral Equations.

In the continuous setting we consider gradient descent

$$\phi^{(n+1)} = \phi^{(n)} + \tau_n p^{(n)}, \tag{2.6}$$

with

$$\tau_n = argmin_{\tau>0} \quad \mathcal{J}(\phi^{(n)} - \tau \nabla_\phi^{H^1}(\phi^{(n)})), \tag{2.7}$$

where τ_n is an optimal step length at iteration n, determined via line-minimization [24]. The conjugate direction $p^{(n)}$ in (2.6) at step n is determined with the Polak-Ribiere method [28]

$$p^{(n)} = -\nabla \mathcal{J}(\phi^{(n)}) + \beta p_{n-1}, \tag{2.8a}$$

$$\beta = \frac{\left\langle \nabla_\phi^{H^1} \mathcal{J}(\phi^{(n)}), \left(\nabla_\phi^{H^1} \mathcal{J}(\phi^{(n)}) - \nabla_\phi^{H^1} \mathcal{J}(\phi^{(n-1)}) \right) \right\rangle_\Gamma}{\left\langle \nabla_\phi^{H^1} \mathcal{J}(\phi^{(n-1)}), \nabla_\phi^{H^1} \mathcal{J}(\phi^{(n-1)}) \right\rangle_\Gamma}, \tag{2.8b}$$

where β is the momentum term, $\langle \cdot, \cdot \rangle_\Gamma$ is an inner product in the Hilbert space $\Gamma = H^1(\Omega)$ and $\nabla_\phi^{H^1}$ is the Sobolev gradient of the functional $\mathcal{J}(\phi)$ with respect to the parameter ϕ. Since $H^1(\Omega) \subset L^2(\Omega)$ this allows us to use either the L^2 inner product $\langle \cdot, \cdot \rangle_{L^2}$ or the Sobolev H^1 inner product $\langle \cdot, \cdot \rangle_{H^1}$ [32]. Here, an L^2 inner product on Ω is used where $\Gamma = L^2(\Omega)$. For quadratic functionals (2.8) coincide with the linear conjugate gradients method [32]. Throughout this thesis, linear problems are considered and the Polak-Ribiere method is employed for the purpose of extending this work to non-linear problems in the future.

2.3 Continous adjoint formulation

By formulating the optimization problem in an adjoint setting, the solution to the adjoint system determines the gradient of the functional [18]. As will be shown, a unique direction for the steepest descent of $\mathcal{J}$ given some perturbation of the boundary data can be extracted from the adjoint system. In the adjoint formulation, $\nabla_\phi \mathcal{J}$ is known as the adjoint sensitivity of $\mathcal{J}$ to the control variable ϕ [18]. To determine the sensitivity $\nabla_\phi \mathcal{J}$, the Gâteaux derivative (also known as the Gâteaux differential) and the Riesz representation theorem are two important concepts.

Definition 2.3.1 (The Gâteaux derivative [3])**.** Let f be a function on an open subset U of a Banach space X into the Banach space Y, f is Gâteaux differentiable at $x \in U$ if there is a bounded and linear operator $T : X \to Y$ such that

$$\lim_{t \to 0} \frac{f(x+th) - f(x)}{t} = T_x(h), \tag{2.9}$$

for every $h \in X$. The operator T is called the Gâteaux derivative of f at x.

The Gâteaux derivative is a generalization of the directional derivative in differential calculus [3] and is required in the continuous formulation. The Gâteaux derivative of (2.3) is

$$\mathcal{J}'(\phi;\phi') = \int_\Omega [u(\phi) - u_{target}]u'(\phi')\ dx\ . \tag{2.10}$$

Theorem 2.3.1 (Riesz representation theorem [26], [32]). *Let H be a Hilbert space, and let $l(x)$ be a bounded linear functional defined on H where $x \in H$. Then $l(x)$ is of the form $l(x) = \langle x, y\rangle_H$ and the point $y \in H$ is uniquely determined. The element y is referred to as the Riesz representer.*

2.3.1 Perturbation in Dirichlet Boundary Condition for Laplace's equation

This thesis deals extensively with interior model problems for Laplace's equation where the boundary data is slightly perturbed. Laplace's equation with a control variable ϕ as Dirichlet data on the boundary Γ is

$$\Delta u = 0, \quad \text{in } \Omega, \tag{2.11a}$$

$$u = \phi, \quad \text{on } \Gamma\ . \tag{2.11b}$$

When the control variable is perturbed by a small perturbation $\phi' \in L^2(\Omega)$ then

$$\phi \leftarrow \phi + \epsilon\phi', \tag{2.12}$$

$$u \leftarrow u + \epsilon u'. \tag{2.13}$$

Substituting these perturbations into (2.11) and collecting $\mathcal{O}(\epsilon)$ terms results in the perturbation system

$$\Delta u' = 0, \quad \text{in } \Omega, \tag{2.14a}$$

$$u' = \phi', \quad \text{on } \Gamma\ . \tag{2.14b}$$

The optimization problem is subjected to the PDE constraint (2.11a)-(2.11b). The adjoint equations are derived by introducing an adjoint variable σ. Multiplying (2.14a) by σ and integrating over Ω

$$0 = \int_\Omega \Delta u'\sigma\ dx, \tag{2.15}$$

and integrating by parts twice on (2.15) results in

$$0 = -\int_\Omega \nabla u' \cdot \nabla\sigma\ dx + \int_\Gamma \frac{\partial u'}{\partial n}\sigma\ ds = \int_\Omega \Delta\sigma u'\ dx - \int_\Gamma \frac{\partial\sigma}{\partial n}u' + \int_\Gamma \frac{\partial u'}{\partial n}\sigma\ ds, \tag{2.16}$$

and with the boundary term in (2.14b) we have that (2.16) simplifies to

$$\int_{\Omega} \Delta\sigma u' \, dx - \int_{\Gamma} \frac{\partial \sigma}{\partial n}\phi' + \int_{\Gamma} \frac{\partial u'}{\partial n}\sigma \, ds = 0 \, . \tag{2.17}$$

Consider the Gâteaux derivative (2.10), by Riesz representation theorem the adjoint sensitivity can be extracted as the unique Riesz representer

$$\mathcal{J}'(\phi;\phi') = \langle \nabla_{\phi}\mathcal{J}, \phi' \rangle_{\Gamma} \, , \tag{2.18}$$

we see that substituting the following adjoint equations

$$\Delta\sigma = [u(\phi) - u_{target}], \qquad \text{in } \Omega, \tag{2.19a}$$

$$\sigma = 0, \qquad \text{on } \Gamma, \tag{2.19b}$$

in (2.17) results in (2.18) where

$$\nabla_{\phi}\mathcal{J} = \frac{\partial \sigma}{\partial n}, \tag{2.20}$$

is the Riesz representer. The optimization problem is a two stage process, first the primal problem (here Laplace's equation) is solved for to determine the state and then the state information is used in the adjoint problem (here Poisson's equation) to determine the descent direction. In this thesis work, this requires a numerical solver for Laplace's equation [2] and a numerical solver for Poisson's equation where the boundary flux of the adjoint variable σ can be extracted [3].

[2] Numerical solvers for Laplace's equation is discussed in Chapter (3).
[3] The adjoint boundary flux is extensively discussed in Chapter (4).

Chapter 3

Boundary Element Methods

3.1 Integral equations

Boundary Integral Equation/s (BIE) are useful tools to convert a PDE defined on some domain Ω into an integral equation that can be solved only on the boundary Γ of Ω. This reduces the dimension of the problem by one order, which simplifies implementation when dealing with domains of arbitrary shape. This is also computationally advantageous as no discretization is needed for the interior points in the domain. In this thesis, the discussion is restricted to 2D-problems, that in the BIE formulation leads to 1D problems. Typically we often encounter situations where either the Dirichlet data U is known on the boundary Γ, the boundary flux $\frac{\partial U}{\partial n}$ is known on Γ or a mixture of the two but not both at the same time.

3.1.1 Fredholm Integral Equation

For a curve Γ in the plane, a (linear) Fredholm equation can be written in terms of complex variables as

$$a(z)\mu(z) + \int_{\Gamma} K(z,\tau)\mu(\tau)\, d\tau = f(z), \quad z \in \Gamma, \tag{3.1}$$

when $a(z) \neq 0\ \forall z \in \Gamma$, the equation is said to be of 2^{nd} kind [29] [1]. $K(z,\tau)$ is called the integral kernel. Fredholm integral equations often arise naturally in physics as the inverse of a differential equation where the integral kernel is a Green's function. Fredholm integral equations of 2^{nd} kind are of particular interest for the purpose of this thesis work as they manifest themselves when formulating Dirichlet problems for Laplace's equation via double layer potentials [2].

[1] In this thesis, only 2^{nd} kind Fredholm integral equations are considered.

[2] Double layer potentials arise in the context of potential theory for elliptic homogeneous boundary value problems. These are discussed in the next section for the indirect BEM for Laplace's equation.

3.1.2 Fredholm's Alternative

For a compact integral operator K that satisfies $K\mu(z) = \int_\Gamma K(z,\tau)\mu(\tau)\, d\tau$, the existence and uniqueness of μ for a 2^{nd} kind Fredholm integral equation $(I+K)\mu = f$ can be determined by Fredholm's Alternative.

Theorem 3.1.1. *(Fredholms's Alternative [29]). If K is a compact linear integral operator from a Banach space X into itself, we have that either $(I+K)\mu = f$ has a unique solution for every $f \in X$, or the homogeneous equation $(I+K)\mu = 0$ has non-trivial solutions.*

3.2 Indirect Boundary Element Method

3.2.1 Derivation of the Indirect Boundary Element Method for Laplace's equation

Interior problem

A central topic in this thesis is the interior Dirichlet boundary value problem for Laplace's equation

$$\Delta U(z) = 0, \qquad z \in \Omega_{int}, \tag{3.2a}$$

$$\lim_{\Omega_{int} \ni \tau \to z} U(\tau) = f(z), \qquad z \in \Gamma, \tag{3.2b}$$

where subscript *int* refers to an interior domain. In order to derive a boundary integral equation one can use either a direct formulation or an indirect approach which is based on potential theory. Following the works of Ojala [29] we use an indirect approach based on potential theory to formulate the Indirect Boundary Element Method (IBEM) for Laplace's equation. For a Dirichlet problem the indirect formulation leads to a Fredholm integral equation of 2^{nd} kind [29], [21]. Some topics from complex analysis are useful in the derivation of the IBEM, in particular analytic/holomorphic functions and Cauchy's integral formula.

Definition 3.2.1 ((Complex-) Analytic function [1])**.** A complex-valued function $f(w)$, $w \in \mathbb{C}$ that is defined on an open set D, is said to be holomorphic if it is complex differentiable at each point of D. Where the complex derivative is defined as

$$f'(w) = \lim_{h \to 0} \frac{f(w+h) - f(w)}{h}, \tag{3.3}$$

where $w \in D$, $w + h \in D$. For $w \in \mathbb{C}$, the term complex-analytic function or holomorphic function is used interchangeably.

In this thesis, the working assumption is that the functions are holomorphic.

Theorem 3.2.1 (Cauchy's integral formula [1]). *Let $D = \{w : |w - w_0| < r\}$ be an open disc with radius r centered at w_0 and let Γ be a closed curve in D, Cauchy's integral formula then states that for any point q not on Γ and in D*

$$f(q) = \frac{1}{2\pi i} \oint_{\Gamma} \frac{f(w)}{w - q}\, dw, \tag{3.4}$$

provided that $f(w)$ is analytic in D.

An immediate result of Theorem (3.2.1) is that for any holomorphic function f that is defined on the disc in the complex plane, for any interior point on the disc the function f can be expressed in terms of boundary values only. The IBEM is formulated by seeking a solution on the form

$$U(z) = \Re\left\{ \frac{1}{\pi i} \int_{\Gamma} \frac{\mu(\tau)}{\tau - z}\, d\tau \right\}, \quad z \in \Omega_{int}. \tag{3.5}$$

For any point $z = \tau \in \Gamma$, the Cauchy type integral in (3.5) cannot be evaluated. However, for any point in the interior we know from Cauchy's integral formula that the integral is analytic. Thus, we consider a point z that approaches the boundary from the interior. For a smooth boundary, if a point $z \in \Omega_{int}$ tends towards a point $\xi \in \Gamma$ then the term inside the brackets in (3.5) tends to the limit [3] [29]

$$U_i(\xi) = \mu(\xi) + \frac{1}{\pi i} \int_{\Gamma} \frac{\mu(\tau)}{\tau - \xi}\, d\tau, \quad \xi \in \Gamma\ . \tag{3.6}$$

Equations (3.2b), (3.5) & (3.6) together leads to a 2^{nd} kind Fredholm integral equation for the density $\mu(z)$

$$\mu(z) + \frac{1}{\pi} \int_{\Gamma} \mu(\tau) \Im\left\{ \frac{d\tau}{\tau - z} \right\} = f(z), \quad z \in \Gamma. \tag{3.7}$$

When the density $\mu(z)$ has been determined on Γ, (3.5) is used to obtain the solution to Laplace's equation for any point $z \in \Omega_{int}$. The most important consequence of equation (3.7) is that we now have an integral equation that is formulated on the boundary only.

Another (equivalent) way of formulating the IBEM is to consider a double layer representation for the density μ. The double layer representation for Laplace's equation is [30]

$$U(x_0) = \frac{1}{2\pi} \int_{\Gamma} \mu(x) \frac{\partial}{\partial n} \log(|x_0 - x|)\, dl(x), \quad x_0 \in \Omega,\ x \in \Gamma, \tag{3.8}$$

where $\mu(x)$ is the dipole density on Γ [30] and $dl(x)$ is the surface measure on Γ. $\frac{1}{2\pi} \log(|x_0 - x|) = G(x, x_0)$ is the Green's function for the free space solution for Laplace's equation. The double layer representation in (3.8) can be

[3] The result in (3.6) is explained by the Sokhotski-Plemelj formulas [29].

transformed into a boundary integral equation of 2^{nd} kind [30]

$$\frac{1}{2}\mu(x_0) + \frac{1}{2\pi}\int_\Gamma \mu(x)\frac{\partial}{\partial n}\log(|x_0 - x|)\, dl(x) = f(x_0), \quad x_0, x \in \Gamma\ . \tag{3.9}$$

By first solving (3.9) for the density μ on the boundary Γ, the solution can then be obtained for any interior point $x_0 \in \Omega$ by solving (3.8). Equation (3.9) rewritten using complex variables simplifies implementation. The corresponding double layer representation in complex variables is [30]

$$\frac{1}{2}\mu(z_0) + \frac{1}{2\pi}\int_\Gamma \mu(z)\Im\left\{\frac{dz}{z - z_0}\right\} = f(z_0), \quad z_0, z \in \Gamma, \tag{3.10}$$

the solution for some point $z_0 \in \Omega$ is obtained by solving

$$U(z_0) = \frac{1}{2\pi}\int_\Gamma \mu(z)\Im\left\{\frac{dz}{z - z_0}\right\}, \tag{3.11}$$

where the density $\mu(z)$ on Γ is known from first solving for $\mu(z)$ in (3.10).

3.2.2 Parametrization and Nyström discretization

We consider the complex double layer representation (3.10). In order to evaluate curve integrals on Γ, the boundary is subdivided into N panels of equal length $h = \frac{2\pi}{N}$, where N is the number of discretization points. The boundary is parameterized with parameter $t \in [0, 2\pi]$ such that $z = z(t)$. Parameterizing (3.10) results in

$$\frac{1}{2}\mu(z_0) + \frac{1}{2\pi}\int_0^{2\pi} \mu(z)\Im\left\{\frac{z'(t)}{z(t) - z_0}\right\} = f(z_0), \tag{3.12}$$

where $\Im$ denotes the imaginary part and superscript $'$ refers to differentiating with respect to t. Equation (3.12) is discretized on the boundary with Nyström discretization

$$\frac{1}{2}\mu(z(t_j)) + \frac{h}{2\pi}\sum_{j=0}^{N-1} \mu(z(t_k))\Im\left\{\frac{z'(t_k)}{z(t_k) - z(t_j)}\right\} = f(z(t_j)), \quad \text{for } j, k = 0, 1, \ldots N-1. \tag{3.13}$$

Equation (3.13) leads to a discrete system of equations

$$\left(\frac{1}{2}\mathbf{I} + \mathbf{K}\right)\vec{\mu} = \vec{f}\,, \tag{3.14}$$

where $\mathbf{I}$ is the $N \times N$ identity matrix and the elements of $\mathbf{K}$ are

$$K_{jk} = \frac{h}{2\pi}\Im\left\{\frac{z_j'}{z_k - z_j}\right\}, \quad j \neq k\ . \tag{3.15}$$

For $j = k$, to avoid division by zero, taylor expansion leads to $K_{jk} = K_{jj} = \Im\left\{\frac{z''(t_j)}{2z'(t_j)}\right\}$ by taking the following limit [29]

$$\lim_{h\to 0} \Im\left\{\frac{z'(t)}{z(t) - z(t+h)}\right\} \approx \Im\left\{\frac{z''(t)}{2z'(t)}\right\}. \tag{3.16}$$

Since we are considering a smooth domain, the kernel is compact and thus by Fredholm's Alternative existence and uniqueness of solutions follows.

Exterior problem

Consider also the exterior problem, where Ω_{ext} is an exterior domain to the boundary curve Γ. The corresponding exterior problem reads

$$\Delta U(z) = 0, \qquad z \in \Omega_{ext}, \tag{3.17a}$$

$$\lim_{\Omega_{ext} \ni z \to \tau} U(z) = f(\tau), \qquad \tau \in \Gamma, \tag{3.17b}$$

$$|U(z)| \leq \lambda, \qquad z \in \Omega_{ext}, \tag{3.17c}$$

the parameter λ is introduced to bound the solution in the far field. In a similar fashion to the interior problem, Helsing and Ojala [21] states that by using the derivation for the exterior problem leads to the boundary integral equation [4]

$$\mu(z) - \frac{1}{\pi}\int_\Gamma \mu(\tau)\Im\left\{\frac{d\tau}{\tau - z}\right\} - 2c_0 = -2f(z), \tag{3.18}$$

where c_0 is a real constant. The discretization is to be performed in the same sense as for the interior problem.

3.2.3 Numerical Approximations to Laplace's Equation on the Unit Disc

Interior problem

To test the IBEM implementation, we consider the interior model problem for Laplace's equation on the unit disc subject to Dirichlet boundary conditions. A sinusoidal Dirichlet boundary condition is used for which an analytic solution is known from the test problem (A.0.2). The problem is

$$\Delta U(z) = 0, \qquad z \in \Omega, \tag{3.19a}$$

$$U(z) = f(z) = 1 + 3\sin(\theta), \qquad z \in \Gamma, \tag{3.19b}$$

where $0 \leq \theta \leq 2\pi$. The analytic solution to (3.19a)-(3.19b) at an interior point $z_0 = r_0 e^{i\theta_0} \in \Omega$ (where subscript $_0$

[4] In this work, a modifed Mihklin representation is used to construct an exterior IBEM for multiply connected domains. Here we only consider one simply connected domain.

denotes an interior domain point) is $U_{ref}(r_0, \theta_0) = 1 + 3r_0 \sin(\theta_0)$ and is here used as the reference solution. The test is performed for $N = 10, 20, \ldots, 100$ discretization points on the boundary. By symmetry of the circle it is only needed to test the IBEM solver at points for a fixed angular direction θ_0 only. However, it is necessary to test at points with different distances r_0 from the origin. This is tested with and without two point linear interpolation, where in the latter case the interpolation is performed by taking the average value of the sum of the exact boundary data and at a point closer to the origin.

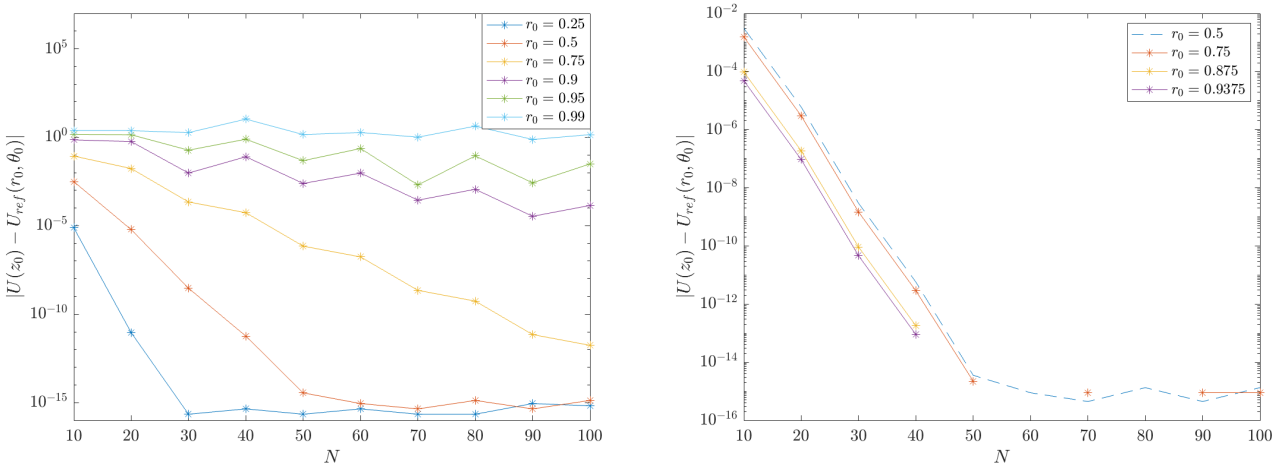

(a) Without two point linear interpolation.

(b) With two point linear interpolation.

Figure 3.1: Pointwise error at different distances r_0 from the origin with $\theta_0 = \pi/4$ with and without utilizing two point linear interpolation. Density $\vec{\mu}$ is computed by Nyström discretization (3.14)-(3.16) and $U(z_0)$ is evaluated with a discretized version of (3.11).

In Figure (3.1a) it is clear that the IBEM performs very well far away from the boundary. Only approximately $N = 30$ points are needed to reach machine precision when $r_0 = 0.25$. However it is clear that as the IBEM approximate solutions close to the boundary, then the error increase. In a IBEM setting, evaluating the solution close to the boundary has shown to be a difficult problem [21]. One simple method for evaluating $U(z_0)$ close to Γ is to interpolate between a boundary value and a solution at a point for which an accurate value can be obtained [21]. Figure (3.1b) shows the error for two-point linear interpolation where the IBEM approximation (without interpolation) at $r_0 = 0.5$ has been used as a reference, subsequent interpolation has been used to obtain the solution at $r_0 = 0.75$, where this approximation is then used as a reference to obtain the approximation at $r_0 = 0.875$ and so on. Comparing the results presented in Figures (3.1a)-(3.1b) it is clear that this simple interpolation method converges faster than without any interpolation.

Exterior problem

The discretization of (3.18) on the unit disc leads to a close to singular system of equations which leads to blow up in the solution. Thus no relevant solution can here be presented. It has been suggested that this could be due to

what is known as a degenerate scale issue [7], [9], [8], [27]. This problem is revisited in Section (3.4).

3.3 Direct Boundary Element Method for Laplace's equation

In this section the pertinent quantity is instead the boundary flux in Laplace's equation. The Direct Boundary Element Method (DBEM) is a mixed method where both the unknown boundary data and the unknown boundary flux can be solved for simultaneously [6]. This is one the advantages of the DBEM. In this setting, the solution procedure is the same if the quantity of interest is either the Dirichlet data, the boundary flux, or a mixure of the two [5].

3.3.1 Derivation of the Direct Boundary Element Method for Laplace's equation

The following method for deriving the DBEM for Laplace's equation is a standard method which can be found in [6], [25]. The DBEM can be derived for any PDE for which we are able to find a fundamental solution. The fundamental solution w for the free space Laplacian in cartesian coordinates satisfies

$$\Delta w + \delta(\xi - x, \eta - y) = 0, \tag{3.20}$$

where $-\infty < x < \infty$, $-\infty < y < \infty$ and δ is the dirac-delta function

$$\delta(\vec{x} - \vec{x_0}) = \begin{cases} 1, & \text{if } \vec{x} = \vec{x_0}, \\ 0, & \text{otherwise.} \end{cases} \tag{3.21}$$

The free space solution for the Laplacian is well known, which in radial coordinates is

$$w = A \ln r + B = -\frac{1}{2\pi} \ln r, \tag{3.22}$$

where B has been set to zero for convenience. The DBEM is derived for Laplace's equation where the fundamental solution w acts as a weight function where the PDE is multiplied by w and then integrated over Ω to find a weak solution

$$\Delta u = 0, \tag{3.23}$$

$$w\,(\Delta u) = 0, \tag{3.24}$$

$$0 = \int_\Omega (\Delta u w)\, d\Omega, \tag{3.25}$$

using the Green-Gauss theorem and integration by parts on (3.25) leads to

[5] The need for solving for the boundary flux in Laplace's equation is discussed in Chapter (4) - Section (4.0.4).

$$\int_\Gamma \frac{\partial u}{\partial n} w \; ds - \int_\Gamma \frac{\partial w}{\partial n} n \; ds + \int_\Omega u \Delta w \; d\Omega = 0, \tag{3.26}$$

and we have the following relation

$$\int_\Omega u \Delta w \; d\Omega = - \int_\Omega u \delta(\xi - x, \eta - y) \; d\Omega = -u(\xi, \eta), \tag{3.27}$$

with ξ,$\eta \in \Omega$. With (3.26) and (3.27) we arrive at the boundary integral equation

$$- \int_\Gamma \frac{\partial u}{\partial n} w \; ds + \int_\Gamma \frac{\partial w}{\partial n} n \; ds + u(\xi, \eta) = 0 \; . \tag{3.28}$$

Under the assumption that $P = (\xi, \eta) \in \Gamma$ and that Γ is smooth [6] at P then (3.28) becomes

$$\frac{1}{2} u(P) + \int_\Gamma u q^* \; ds = \int_\Gamma u^* \frac{\partial u}{\partial n} \; ds, \tag{3.29}$$

where $u^* = w$ is the fundamental solution to Laplace's equation and $q^* = \frac{\partial w}{\partial n}$ is the corresponding boundary flux, u and q are the solution variables. Now, the original PDE has been transformed into an integral equation in terms of integrals over the boundary only.

3.3.2 Discretization of the Direct Boundary Element Method

For the 2D Laplace's equation, the discretized boundary integral equation is found by subdividing the boundary into N segments. In the simplest case each element have a node at its center and the solution variables are set to be constant on each elements (thus the solution is discontinuous over the boundary). By considering a single point i on the boundary, discretization of (3.29) leads to [25]

$$\frac{1}{2} u_i + \sum_{j=1}^{N} \int_{\Gamma_j} q^* u \; d\Gamma = \sum_{j=1}^{N} \int_{\Gamma_j} u^* q \; d\Gamma. \tag{3.30}$$

When considering all points on the boundary, the discretization (3.30) leads to a linear system of equations on the form $Hu = Gq$ [25]. When solving for the boundary flux q only, the Dirichlet data u must be known on the entire boundary. Several authors suggest that the influence coefficients [7] in the $G \rightarrow \int_{\Gamma_j} u^* q \; d\Gamma$ and $H \rightarrow \int_{\Gamma_j} q^* u \; d\Gamma$ matrices can be determined analytically by exact boundary element integrations utilizing Gauss-Legendre quadrature with either zeroth order, linear or quadratic polynomials [13], [14]. This is the method of choice in present work since this will be shown to also translate to solving Poisson's equation with the DBEM [14]. It should be noted that special care has to be taken for the diagonal entries since the integrands are singular at these points.

[6] The factor $\frac{1}{2}$ in (3.29) only holds for when Γ is smooth at P. This is the only case considered in this work.
[7] The terms H_{ij} and G_{ij} are known as influence coefficients.

3.4 Shortcomings for Boundary Element Methods and their Remedies

The following section discuss some of the frequently discussed disadvantages of Boundary Element Methods and solution strategies to alleviate some of these problems. With the method outlined in [13] the test problem (A.0.2) has been used to compute the boundary flux and to compare this to the analytical solution. The results are not satisfactory. It is unclear if the erroneous results are due to implementation error, or if there is another underlying issue. Possible issues are degenerate scale issues.

3.4.1 Degenerate Scale and the Unit Circle Trap

It is noted that BEMs sometimes exhibit a problem known as degenerate scale for Dirichlet problems which shows up with regular shapes for Poisson's equation and Laplace's equation [7], [9], [27], [33]. This manifests itself as rank deficiency and close to singular matrices that are causing blow up or non-unique solutions, even if well-posedness of the underlying PDE is satisfied. The problem can occur for irregular shapes as well but is more prevalent for symmetric geometries, in particular this occurs for the unit disk [33]. For the unit disc the term "The Unit Circle Trap" is often used to refer to this degenerate scale issue [8]. The problem is due to difficulties in implementation and programming while BEMs on their own predicts correct solutions. This is known in the BEM community and is also a problem in commercial BEM codes [9]. It should be noted that both the indirect formulation and the direct formulation are susceptible to degenerate scaling issues and that the character of the issue is different depending on the method [8]. For the indirect approach this has been shown to occur for exterior problems and for the direct approach this can occur for the interior problems. In [8], Chen et. al makes arguments based on Fredholm's Alternative that the DBEM and IBEM are not equivalent in their solution spaces and the occurrence of degenerate scale issues is dependent on the choice of method. The degenerate scale problem turns out to be a good candidate to explain the erroneous result obtained in the preceding sections for solving Laplace's equation with Dirichlet boundary data. It should be noted that this might not be a problem in practical applications when working with irregular domains but it is indeed troublesome for testing purposes and validation.

3.4.2 Exterior and Interior Problems Revisited: The Kelvin Transformation

With the indirect approach it is possible to solve for the interior Dirichlet problem for Laplace's equation. However, IBEM might be facing a degenerate scale issue for the corresponding exterior problem. For this reason we consider a method of transforming an exterior problem into an equivalent interior problem, namely the Kelvin transformation. This allows us, for the exterior problem, to use the easier to implement interior solver based on the indirect approach. An exterior Dirichlet problem can be transformed into an equivalent interior Dirichlet problem via the

[8] A good description on why this occurs for the unit circle is given in [33].

Kelvin transformation [2]. The exterior Dirichlet problem

$$\begin{aligned} \Delta u(x,y) &= 0, && (x,y) \in \Omega_{ext}, \\ u(x,y) &= f(x,y), && (x,y) \in \Gamma, \\ \lim_{r\to\infty} \sup_{|(x,y)|\geq r} |u(x,y)| &< \infty, \end{aligned}$$

transforms into the interior Dirichlet problem [2]

$$\begin{aligned} \Delta \hat{u}(\xi,\eta) &= 0, && (\xi,\eta) \in \Omega_{int}, \\ u(\xi,\eta) &= f(T^{-1}(\xi,\eta)), && (\xi,\eta) \in \hat{\Gamma}\ , \end{aligned}$$

where $\hat{u}(\xi,\eta) = u(x,y)$ and $\hat{\Gamma}$ is the boundary of $\Omega_{int} = T(\Omega_{ext})$ and the Kelvin transformation is defined as

$$T(x,y) = (\xi,\eta) = \frac{1}{r^2}(x,y), \quad r = \sqrt{x^2+y^2}\ \ .$$

The Kelvin transformation is an involutory function $T(T(x,y)) = (x,y)$ and $T^{-1} = T$ where (ξ,η) is the inverse of (x,y) with respect to the unit circle [2]. If one seeks to solve the exterior problem it is recommended to make use of the transformation and then use the interior Laplace solver thus circumventing the issue of singular matrices for the IBEM with exterior problems.

3.5 GMRES and FMM

Another disadvantage of BEMs that is well known in the community is that discretization of BIE leads to full matrices. This is due to the non-local structure of the discretizations as opposed to discretizations with Finite Element Method (FEM), Finite Difference Method (FDM) or Finite Volume Method (FVM) that can exploit the local nature of the methods to create sparse matrices. The non-sparsity of the matrices have negative implications on computation time. Typically Generalized Minimal Residual Method (GMRES) [29] is used to solve the linear systems that arise from the BEM discretization to accelerate computation. It should be noted that, in order for BEMs to be competitive with respect to computation time, the Fast Multipole Method (FMM) would be employed together with GMRES [29].

Chapter 4

Estimation of the Adjoint Normal Derivative

This chapter is devoted to finding methods of estimating the Riesz representer (2.20) where we consider the adjoint system (2.19).

4.0.1 The κ-test

The κ-test is crucial for testing and validation of the numerical solvers in order to verify the validity of (2.18). For any arbitrary perturbation ϕ', the Gâteaux derivative (2.10) and with the adjoint normal derivative (2.18), (2.20) being the Riesz representer, we define κ as [28]

$$\kappa := \frac{\mathcal{J}'(\phi;\phi')}{\left\langle \frac{\partial \sigma}{\partial n}, \phi' \right\rangle_{\Gamma}}. \tag{4.1}$$

When κ is close to 1 for any arbitrary perturbation ϕ', this suggests that the numerical solver estimates the Riesz representer correctly. This test can also give insights on the how the error manifests itself depending on the numerical solver used.

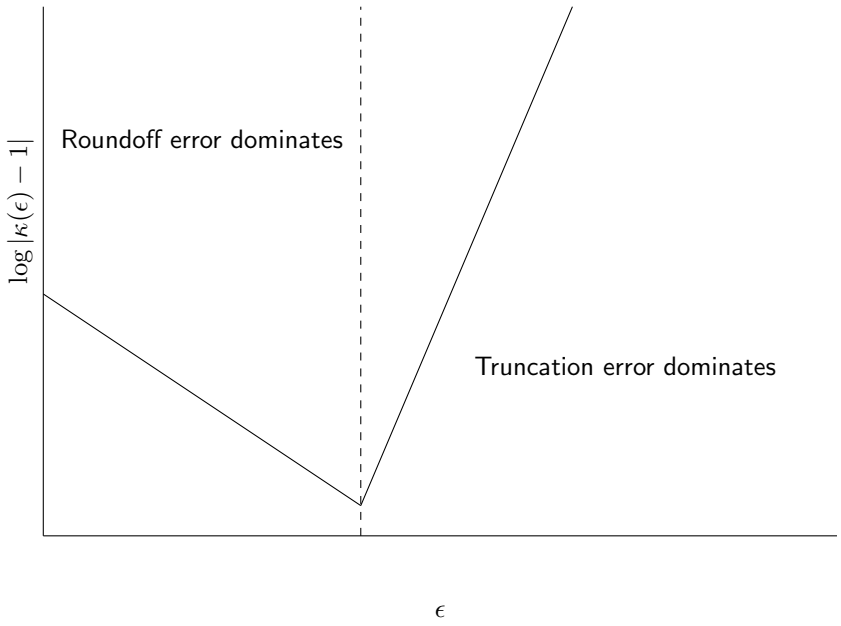

Figure 4.1: Conceptual drawing of a κ-test.

Typically it is expected that the κ-test will show regions where the round off error dominates and another region where the truncation error dominates. It is expected that as parameters in the model are refined (for instance by increasing the number of discretization points in the BEM) the error should decrease overall.

4.0.2 The Poisson Kernel Method

The adjoint equations (2.19a)-(2.19b) can be written on the form

$$\Delta\sigma + V\sigma = f, \qquad \text{in } \Omega, \tag{4.2a}$$

$$\sigma = g_D, \qquad \text{in } \Gamma, \tag{4.2b}$$

where $V \equiv 0$ and $\sigma = g_D = 0$ on Γ. The normal derivative at any coordinate point $a \in \Gamma$ exists and $\frac{\partial\sigma(a)}{\partial n} > 0$ [31]. The solution $\sigma \in \Omega$ and the corresponding point-wise normal derivative at a coordinate point $a \in \Gamma$ for this problem is obtained by

$$\sigma(x) = \int_\Omega G(x,y)\Delta\sigma(y)\, dy, \tag{4.3a}$$

$$\frac{\partial\sigma}{\partial n}(a) = \int_\Omega K(a,y)\Delta\sigma(y)\, dy, \tag{4.3b}$$

where $K := \frac{\partial G}{\partial n}$ is the Poisson kernel of Δ in Ω [31]. For a ball in $\mathbb{R}^n$ with radius R the Poisson kernel is

$$K(a,y) = \frac{1}{n\omega_n R}\frac{R^2 - |y|^2}{|a-y|^n}, \tag{4.4}$$

where n is the dimension of the problem, ω_n is the surface area of the n-ball and a, y are points in Ω [11]. For evaluation of the integral in (4.3b), a is a fixed point on the boundary Γ. Numerical evaluation of the integrals in equation (4.3b) typically needs some quadrature rule for general domains. However, when the domain Ω is a ball in $\mathbb{R}^n$ there are some special quadrature identities that simplify the integration greatly. In this regard, holomorphic functions (Definition (3.2.1)), harmonic functions, subharmonic functions as well as quadrature domains will be useful to consider. Since this thesis considers 2-dimensional problems only, the following discussion is restricted to the particular case where the ball is in $\mathbb{R}^2$, that is, a Ω is disc with radius R. However, it should be noted that much of the following can be generalized for $n > 2$.

A real valued and continuous function $u(x, y)$ defined on Ω is harmonic if it satisfies Laplace's equation: $\Delta u = u_{xx} + u_{yy} = 0$ [1]. In addition, by linearity of Laplace's equation, the sum of two harmonic functions is another harmonic function [1]. Moreover, a harmonic function $u \in \Omega$ is a holomorphic function in Ω.

Definition 4.0.1 (Quadrature identities on the disc [4])**.** On a unit disc centered at the origin (here denoted as $D_1(0)$ with its boundary $bD_1(0)$), any holomorphic function h satisfy the following quadrature identities,

$$\pi h(0) = \iint_{D_1(0)} h \; dA, \tag{4.5a}$$

$$2\pi h(0) = \int_{bD_1(0)} h(z) \; ds. \tag{4.5b}$$

The disc is the simplest example of what is known as a quadrature domain, and often harmonic functions are used as test functions on the disc [19]. It has been shown that discs are the only domains that satisfy such a simple quadrature identity [19]. Since the area of a disc with radius R is known, evaluating the integral for a fixed point $a \in \Gamma$ in equation (4.3b) only amounts to computing the integrand at the center of the disc, i.e. $y = y_0 = 0$, and multiplying by the area $|\Omega| = \pi R^2$ of the disc. Thus the point-wise normal derivative at $a \in \Gamma$ is obtained as

$$\frac{\partial \sigma}{\partial n}(a) = \pi R^2 K(a, y_0)\Delta\sigma(y_0) = \pi R^2 \frac{1}{2\pi R}\frac{R^2 - |y_0|^2}{|a - y_0|^2}\Delta\sigma(y_0) = \frac{R}{2}\frac{R^2}{|a|^2}\Delta\sigma(0) = \frac{R}{2}\Delta\sigma(0) \; . \tag{4.6}$$

It is noted that, the normal derivative has the same magnitude for all $a \in \Gamma$ since $|a| = R$ for $a \in \Gamma$. In the particular case where Ω is the unit disc ($R = 1$) with its center at the origin $y_0 = 0$, equation (4.6) simplifies to $\frac{\partial \sigma}{\partial n}(a) = \frac{1}{2}\Delta\sigma(0)$. In the following sections we will consider the unit disc $R = 1$. From the adjoint system (2.19) it is known that $\Delta\sigma(y) = [u(y, \phi) - u_{target}(y, \phi)]$, for $y \in \Omega$. The magnitude of the point-wise normal derivative at any point $a \in \Gamma$ is then

$$\frac{\partial \sigma(a)}{\partial n} = \frac{[u(0, \phi) - u_{target}(0, \phi)]}{2}, \tag{4.7}$$

and when the magnitude of $\frac{\partial \sigma(a)}{\partial n}$ is constant on Γ then

$$\left\langle \frac{\partial \sigma}{\partial n}, \phi'(z) \right\rangle_{\Gamma} = \frac{[u(0,\phi) - u_{target}(0,\phi)]}{2} \int_{\Gamma} \phi'(z)\, dz. \tag{4.8}$$

In the following sections, (4.8) is to be determined for some different perturbations ϕ' in (2.14b) to the boundary data (2.11b) and corresponding κ-tests are carried out. For the rest of this chapter, if not otherwise stated, the boundary data (2.11b) is set to a constant $\phi = 1$ and the state variable u is computed with the interior IBEM Laplace solver developed in section (3.2). The target solution is solved with the same numerical solver where $u_{target} = u(\widehat{\phi})$ and $\widehat{\phi}$ is determined by (2.4) where z_p is determined by (2.5).

Constant perturbation data

On the unit circle, for a constant perturbation ϕ', equation (4.8) is

$$\left\langle \frac{\partial \sigma}{\partial n}, \phi' \right\rangle_{\Gamma} = \frac{[u(0,\phi) - u_{target}(0,\phi)]}{2} 2\pi\phi' = \pi\phi' \left[u(0,\phi) - u_{target}(0,\phi)\right] \ . \tag{4.9}$$

To test the validity of this expression, a κ-test is performed. For this, the functional has to be evaluated. Consider a harmonic function $w(\phi)$ defined on Ω and define the functional $\mathcal{J}$ as

$$\mathcal{J}(w(\phi)) := \frac{1}{2} \int_{\Omega} w(\phi)^2 dx \ , \tag{4.10}$$

the Gâteaux derivative (2.9) of (4.10) is

$$\mathcal{J}'(\phi;\phi') = \lim_{\epsilon \to 0} \frac{\mathcal{J}\left(w(\phi) + \epsilon w'(\phi')\right) - J\left(w(\phi)\right)}{\epsilon} = \frac{d}{d\epsilon} \mathcal{J}\left(w(\phi + \epsilon\phi')\right)\big|_{\epsilon=0} = \int_{\Omega} w(\phi) w'(\phi')\, dx, \tag{4.11}$$

let Ω be a circle with radius R, with a constant perturbation ϕ', $w'(\phi') = \phi'$ is constant on Ω and the term $w(\phi)w'(\phi')$ satisfies the first quadrature identity (4.5a) since the integrand is harmonic and the Gâteaux derivative simplifies to

$$\mathcal{J}'(\phi;\phi') = \pi R^2 \left(w(0,\phi) w'(\phi')\right). \tag{4.12}$$

The numerical result with a random exterior domain point z_p (as defined by (2.5)) where $u_{target} = u(\widehat{\phi})$ (with $\widehat{\phi}$ defined by (2.4)) close to the boundary is plotted. The point is chosen such that $\theta = \theta_{rnd} \in [0, 2\pi]$ is determined randomly with MATLABs `randn` command. The κ-test is presented in Figure (4.2).

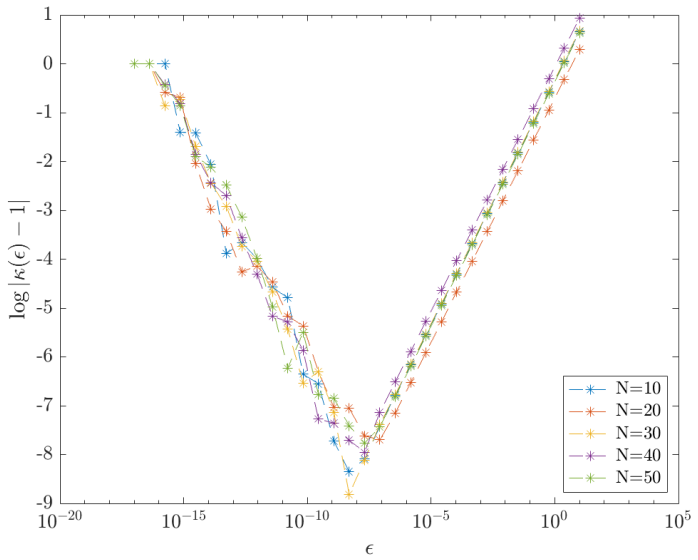

Figure 4.2: κ-test with constant perturbation $\phi' = 1.01$ for a random exterior point $z_p = R_{ext}e^{i\theta_{rnd}}$ with $R_{ext} = 1.01$.

The results in Figure (4.2) corresponds well with the conceptual drawing of the κ-test in Figure (4.1). When $\epsilon \lessapprox 10^{-8}$ the roundoff error dominates and when $\epsilon \gtrapprox 10^{-8}$ then the truncation error dominates. Moreover, the results in Figure (4.2) support the claim that the quadrature identities (4.5a)-(4.5b) holds for the unit circle. Since the perturbation is constant on the boundary, by the strong maximum principle for harmonic functions the solution to the perturbed problem is constant in Ω [11]. With this in mind, any point other than $y = y_0 = 0$ in Ω could have been chosen as the test point and have shown qualitatively similar result for the κ-test. Thus it is vital to demonstrate that the quadrature identities holds for any random perturbation.

Arbitrary perturbation

For any arbitrary perturbation $\phi' = \phi'(z)$ over the boundary Γ, the integral in equation (4.8) is

$$\int_\Gamma \phi'(z)dz = 2\pi R \cdot \overline{(\phi'(z))} \text{ [35]},$$

where $\overline{(\phi(z))}$ denotes the average of $\phi'(z)$ over Γ. κ is

$$\kappa(\epsilon) = \lim_{\epsilon \to 0} \frac{\frac{\mathcal{J}(\phi+\epsilon\phi') - \mathcal{J}(\phi)}{\epsilon}}{\left\langle \frac{\partial \sigma}{\partial n}, \phi'(z) \right\rangle_\Gamma}, \tag{4.13}$$

where we consider the Gâteaux derivative (4.11). The integrand in equation (4.10) is the square of a harmonic function. The square of a harmonic function is a subharmonic function. A necessary and sufficient condition for a function $u \in \Omega$ to be subharmonic function is for u to have a positive Laplacian $\Delta u \geq 0$ [1]. On the disc in $\mathbb{R}^2$ it holds that subharmonic functions are holomorphic functions. An immediate consequence to this is that a subharmonic function on the disc in $\mathbb{R}^2$ will satisfy the quadrature identities (4.5a)-(4.5b). Thus, the method

of evaluating the functional at the circle center is still valid. This hypothesis is tested by another κ-test. The corresponding numerical result for equation (4.13) for a random perturbation is presented in Figure (4.3). The perturbation vector $\phi'(z)$ is chosen randomly with MATLABs built in `randn` command such that at every point $z \in \Gamma$, $\phi'(z) \in [0.8, 1.2]$ is determined randomly between 0.8 and 1.2.

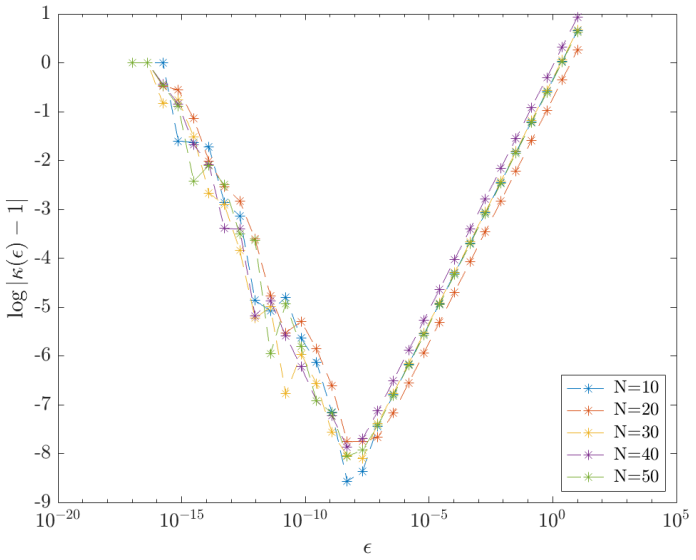

Figure 4.3: κ-test for a random perturbation $\phi'(z)$ with a random exterior point $z_p = R_{ext}e^{i\theta_{rnd}}$ in u_{target} with $R_{ext} = 1.01$.

The result in Figure (4.3) indeed show that when evaluating the functional at the center as well as when evaluating the integrand in equation (4.6) the results are satisfactory. It is worth noting that accuracy does not increase as parameters are refined. While these results are good, as only circles have the simple quadrature identities these results may not hold for general domains. Since the motivation is to extend this work to general domains, there is a need to develop numerical methods for evaluating these integrals. Typically, numerical quadrature to evaluate the integrals in (4.3b) is often employed for this purpose.

Pointwise δ-κ-test for an arbitrary perturbation

Before moving on to the numerical quadrature, it is good to test how well a κ-test will perform at other points than the origin. As is known from the formulation of BIE in Chapter (3) from the results in Figure (3.1a), the error increase close to the boundary, thus it is of interest to see how the κ-test fares for points further away from the origin. By symmetry of the circle, θ is fixed and only the distance from the origin is tested here. Let δ denote the Dirac-delta function (3.21) and define an operator H which utilizes the "sifting" property of the Dirac-delta function, such that

$$Hu := \int_\Omega \delta(x - x_0)u(x, \phi)\ dx = u(x_0, \phi). \tag{4.14}$$

The functional is rewritten in a point-wise sense as

$$\mathcal{J}(u(\phi)) = \frac{1}{2}\int_\Omega \left[u(x,\phi) - u_{target}(x)\right]^2 dx = \frac{1}{2\pi}\int_\Omega \left[Hu(x,\phi) - Hu_{target}(x)\right]^2 dx = \frac{1}{2}\left[u(x_0,\phi) - u_{target}(x_0)\right]^2, \tag{4.15}$$

computing the Gâteaux derivative (2.9) at x_0

$$\mathcal{J}'(\phi;\phi') = \frac{d}{d\epsilon}\mathcal{J}\left(u(\phi + \epsilon\phi')\right)\Big|_{\epsilon=0} = \left[u(x_0,\phi) - u_{target}(x_0)\right]u'(x_0,\phi'), \tag{4.16}$$

and this point-wise notion applied to the normal derivative in (4.3b) evaluates to

$$\begin{aligned}
\frac{\partial\sigma(a)}{\partial n} &= \int_\Omega K(a,x)\left[u(x,\phi) - u_{target}(x)\right]\ dx = \frac{1}{2\pi}\int_\Omega \delta(x-x_0)K(a,x)\left[u(x,\phi) - u_{target}(x)\right]\ dx \\
&= K(a,x_0)\left[u(x_0,\phi) - u_{target}(x_0)\right] = \frac{1}{2\pi}\frac{1-|x_0|^2}{|a-x_0|^2}\left[u(x_0,\phi) - u_{target}(x_0)\right] \\
&= \frac{1}{2\pi}\frac{1-|x_0|^2}{1+|x_0|^2 - 2|x_0|\,cos(\theta - \theta_{x_0})}\left[u(x_0,\phi) - u_{target}(x_0)\right],
\end{aligned} \tag{4.17}$$

with $a = e^{i\theta} \in \Gamma$ and $x_0 = r_0 \cdot e^{i\theta_{x_0}} \in \Omega$, $0 \leq r_0 < 1$. It should be noted that when

$$\theta = \arccos\left(\frac{1+|x_0|^2}{2|x_0|}\right) + \theta_{x_0}, \tag{4.18}$$

then we have division by zero in (4.17). Numerical results for (4.17) for constant Dirichlet data ϕ gives the following results for the normal derivative.

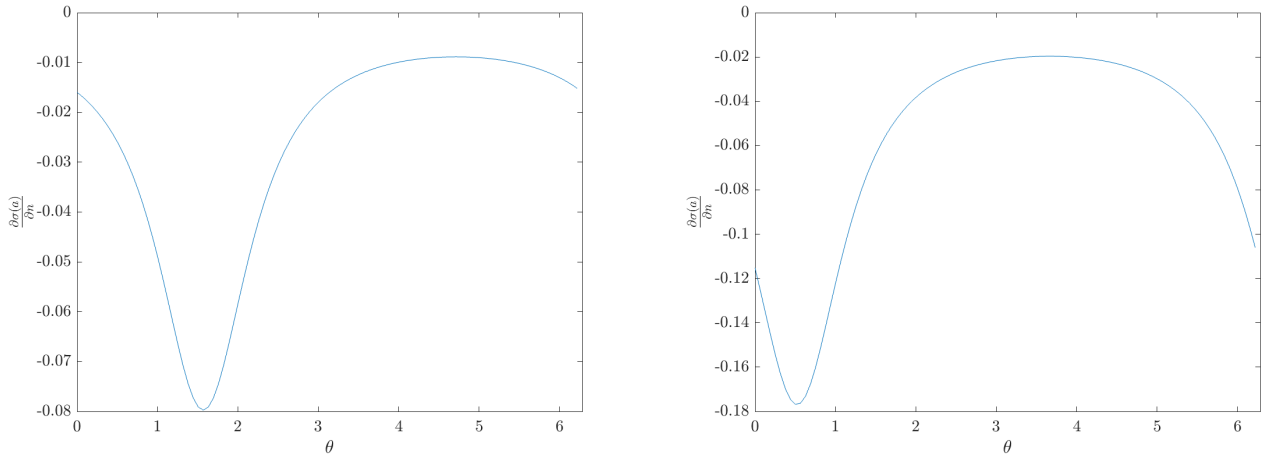

(a) $x_0 = 0.5 \cdot e^{i\pi/2}$.

(b) $x_0 = 0.5 \cdot e^{i\pi/6}$.

Figure 4.4: Computing the last term in (4.17) to evaluate $\frac{\partial\sigma(a)}{\partial n}$ pointwise on the unit disc for different $a = e^{i\theta}$ where $\theta \in [0, 2\pi)$. A fixed x_0 is used and constant Dirichlet data $\phi = 1$ in (2.11b) is used. State variable u is computed by solving Laplace's equation (2.11a)-(2.11b) with the interior IBEM solver developed in section (3.2). $\phi(z)$ denotes the Dirichlet data in (2.11b). Here, we consider a point z_p in (2.5) & (2.4) far away from the boundary such that $u_{target} = 0$.

r_0	θ_{x_0}	$\Re\left\{\arccos(\frac{1+\lvert x_0\rvert^2}{2\lvert x_0\rvert}) + \theta_{x_0}\right\}$
0.5	$\pi/2$	1.57
0.5	$\pi/6$	0.52

Table 4.1: Problematic angles as defined by (4.18) for $x_0 = r_0 \cdot e^{i\theta_{x_0}}$.

In Figure (4.4) and the corresponding Table (4.1) this dependence on the angle θ is seen. In Figure (4.4) the angle θ at which the spikes in the normal derivative occur corresponds with the real part of equation (4.18). Clearly, the results in Figure (4.4) does not correspond to the analytical solution for the normal derivative to σ from test problem (A.0.3) which should be constant for all θ with a value of $\frac{1}{2}$.

Results $\kappa - \delta$-test: The $\kappa - \delta$ tests is performed for a fixed $\theta_{x_0} = \pi/3$ for 4 different distances r_0 from the origin, $r_0 = 0, 0.5, 0.75$ and 0.99. Again, the exterior point z_p (2.5) is chosen to have the radius $R_{ext} = 1.01$ with a randomized $\theta \in [0, 2\pi]$.

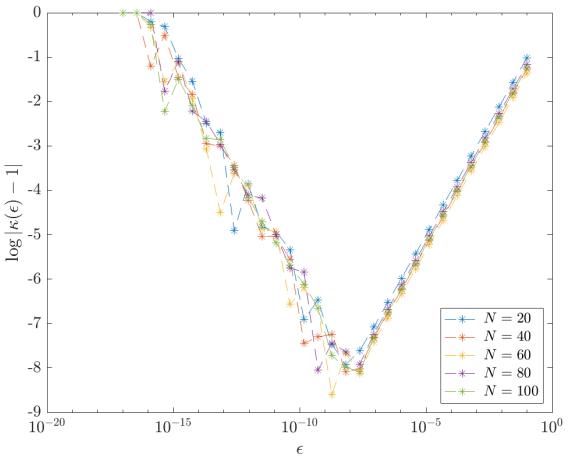

(a) κ-test with $x_0 = 0$.

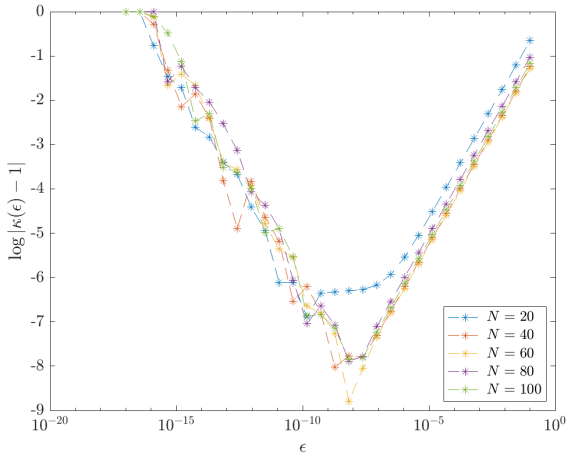

(b) κ-test with $x_0 = 0.5e^{i\pi/3}$.

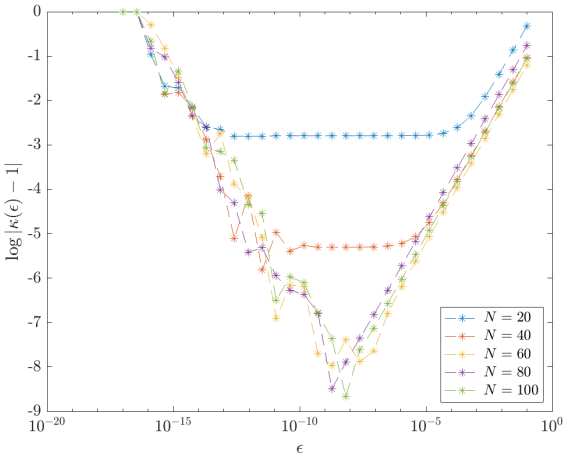

(c) κ-test with $x_0 = 0.75e^{i\pi/3}$.

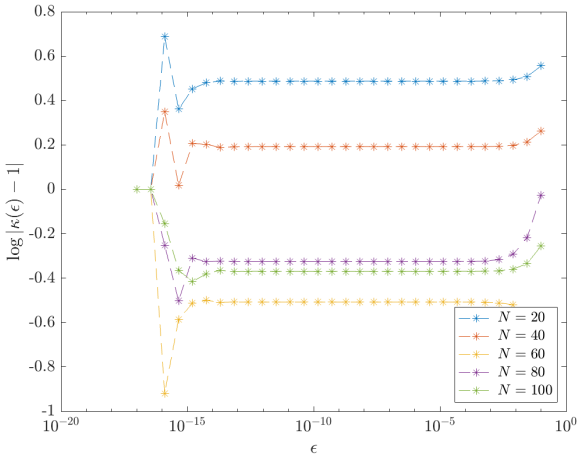

(d) κ-test with $x_0 = 0.99e^{i\pi/3}$.

Figure 4.5: Point-wise κ-δ-test for a fixed angle $\theta_{x_0} = \frac{\pi}{3}$ for 4 different distances r_0 from the origin where $x_0 = r_0 e^{i\theta_{x_0}}$ and a random exterior point $z_p = R_{ext} e^{i\theta_{rnd}}$ in u_{target} with $R_{ext} = 1.01$.

From the results in Figure (4.5) we see that for a fixed N, further away from the origin, the results are no longer precise and this effect is larger the further away from the origin the point x_0 is. For a fixed $x_0 \neq 0$, as N increase, $\log|\kappa(\epsilon) - 1|$ decrease which is expected since the approximation of $\nabla_\phi \mathcal{J}$ should be more accurate as parameters are refined.

Numerical quadrature on the unit disc

For the integral in equation (4.3b) for the normal derivative as well as for evaluating the functional on the form (4.10), n-point Gauss-Legendre quadrature in polar coordinates is used to evaluate double integrals. That is, n quadrature nodes in the radial direction as well as n quadrature nodes in the angular direction. The Gauss-Legendre quadrature for a function $f(x)$ is

$$\int_{-1}^{1} f(x)\ dx \approx \sum_{i=1}^{n} w_i f(x_i), \tag{4.19}$$

where w_i are weights determined by the n-point quadrature rule. The integrals considered here are for $0 \leq r \leq 1$ and $0 \leq \theta \leq 2\pi$ so the integration limits has to be changed in order to be on the form (4.19), the following change in limits can be performed

$$\int_{a}^{b} f(x)\ dx \approx \frac{b-a}{2} \sum_{i=1}^{n} f\left(\frac{b-a}{2}\xi_i + \frac{a+b}{2}\right), \tag{4.20}$$

where ξ_i are integration points determined by the n-point quadrature rule. Now, (4.20) is equivalent to (4.19). For the following analysis, consider $n = 3$, with the weights 1, 2 and 1 the corresponding quadrature nodes at $-\sqrt{3/5}$, 0 and $\sqrt{3/5}$. With $z_0 = re^{i\theta}$, let $f(z_0) = u(r,\theta,\phi) - u_{target}(r,\theta,\phi)$. Recall from (3.11) that

$$U(z_0) = \frac{1}{2\pi} \int_{\Gamma} \mu(z) \Im\left\{\frac{dz}{z - z_0}\right\},$$

and define $U(r,\theta) := U(z_0)$. The normal derivative on the unit disc at a fixed point $a = e^{i\theta_a} \in \Gamma$ is obtained by integrating in the radial direction r and the angular direction θ

$$\begin{aligned} \frac{\partial \sigma}{\partial n}(a) &= \int_{\Omega} K(a,y)\Delta\sigma(y)\ dy = \int_{r=0}^{1} \int_{\theta=0}^{2\pi} (K(a,r,\theta)(u(r,\theta,\phi) - u_{target}(r,\theta,\phi))) \cdot r\ d\theta dr \\ &\approx \frac{\pi}{2} \sum_{j=1}^{n=3} w_j \sum_{i=1}^{n=3} w_i K(a,\zeta_j,\xi_i) \cdot U(\zeta_j,\xi_i) \cdot \zeta_j, \end{aligned} \tag{4.21}$$

with w_i, w_j and ξ_i and ζ_j being the weights are corresponding quadrature nodes for 3-points Gauss-Legendre quadrature. The Gauss-Legendre approximations for the functionals on the form in (4.10) are obtained in a similar fashion. The results for the approximation of the normal derivative are presented in Figure (4.6).

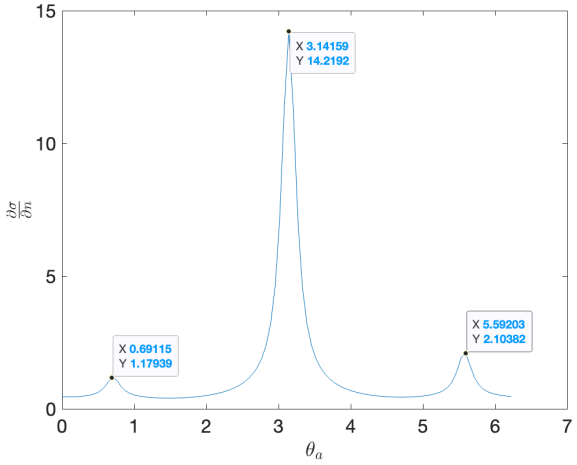

(a) Computation of the adjoint normal derivative (4.21) with data $\phi(z) = 1$ with random perturbation $\phi'(z)$ and random exterior point $z_p = R_{ext}e^{i\theta_{rnd}}$ where $R_{ext} = 1.01$ and $\theta_{rnd} \in [0, 2\pi]$.

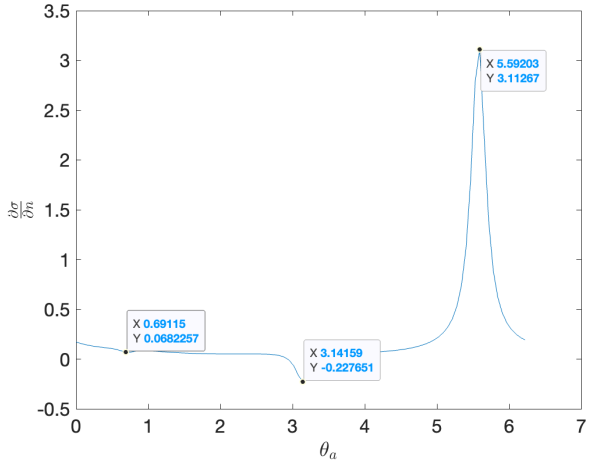

(b) Computation of the adjoint normal derivative (4.21) with random data $\phi(z)$. The data $\phi(z)$ is chosen randomly with MATLABs built in `randn` command such that at every point $z \in \Gamma$, $\phi'(z) \in [0.8, 1.2]$ is determined randomly between 0.8 and 1.2. A random perturbation $\phi'(z)$ is used and a random exterior point $z_p = R_{ext}e^{i\theta_{rnd}}$ where $R_{ext} = 1.01$ and $\theta_{rnd} \in [0, 2\pi]$.

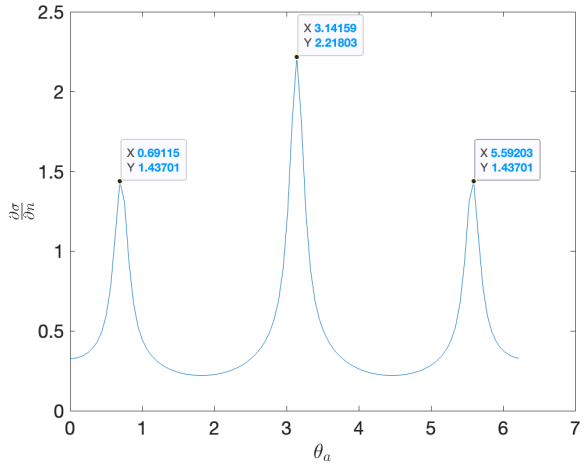

(c) Computation of the adjoint normal derivative (4.21) with data $\phi(z) = 1$ with random perturbation $\phi'(z)$ and random exterior point $z_p = R_{ext}e^{i\theta_{rnd}}$ far away from the boundary with $R_{ext} = 10^{13}$ and $\theta_{rnd} \in [0, 2\pi]$.

Figure 4.6: Computation of the adjoint normal derivative (4.21) on the unit disc at fixed points $a = e^{i\theta_a}$, for multiple values of $\theta_a \in [0, 2\pi)$ with Gauss-Legendre quadrature. State variables u and u_{target} is computed by solving Laplace's equation (2.11a)-(2.11b) with the interior IBEM solver developed in section (3.2). $\phi(z)$ denotes the Dirichlet data in (2.11b) and $\phi'(z)$ denotes the perturbation (2.14b). The perturbation vector $\phi'(z)$ is chosen randomly with MATLABs built in `randn` command such that at every point $z \in \Gamma$, $\phi'(z) \in [0.8, 1.2]$ is determined randomly between 0.8 and 1.2. For $u_{target} = u(\widehat{\phi})$, $\widehat{\phi}$ is determined by (2.4) and z_p is defined by (2.5).

For Dirichlet data $\phi = 1$ in (2.11b) and with an exterior point where $R_{ext} \to \infty$ in (2.5) we have an integration over Ω where the integrand is the Poisson kernel. For constant Dirichlet data and with $u_{target} \to 0$ the results in Figure (4.6) does not agree with the analytic solution (A.5) for the boundary flux which is $\frac{1}{2}$ when $B_0 = 1$ and $R = 1$. It should also be noted that the spikes in the normal derivative occur at the same angles when the problem

has random Dirichlet data. Moreover, these spikes remain when z_p is set far away from the boundary. Thus this suggests that these spikes in the normal derivative are not due to influence of the target solution.

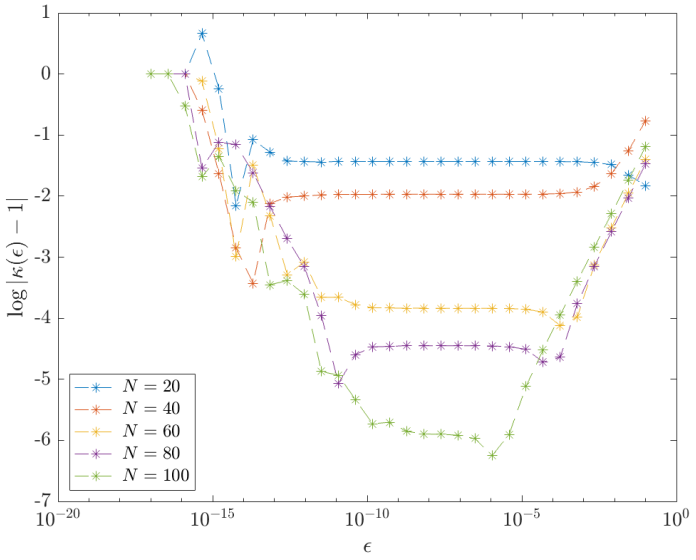

Figure 4.7: κ-test constant Dirichlet data $\phi = 1$, a random perturbation $\phi'(z)$, and random exterior point $z_p = R_{ext}e^{i\theta_{rnd}}$ with radius $R_{ext} = 1.01$. This κ-test corresponds to the results for $\frac{\partial\sigma}{\partial n}$ presented in Figure (4.6a).

The results in Figure (4.7) for the κ-test show that the error in the approximations to the normal derivative goes down as the number of discretization points N on the boundary increase. However, considering the erroneous results in Figure (4.6a), this suggests that integrating Poisson type kernels with Gauss-Legendre quadrature yields nonphysical results in the approximation of the normal derivative and a successful κ-test alone is not sufficient for the approximation to be valid. For this reason, this issue has to be treated to avoid these spikes or another method altogether should be used to compute the normal derivative.

4.0.3 The Directional derivative approach

The adjoint system (2.19a)-(2.19b) is of the form

$$\Delta\sigma(\mathbf{x}) = f, \quad \mathbf{x} \in \Omega, \tag{4.22a}$$

$$\sigma(\mathbf{x}) = 0, \quad \mathbf{x} \in \Gamma\ . \tag{4.22b}$$

By definition, the normal derivative is found to be the directional derivative in the normal direction to the boundary

$$\frac{\partial\sigma}{\partial n}(\mathbf{x}) = \lim_{h\to 0}\frac{\sigma(\mathbf{x}+h\mathbf{n}) - \sigma(\mathbf{x})}{h}, \quad \mathbf{x} \in \Gamma. \tag{4.23}$$

With (4.22b) for the adjoint problem, this simplifies to

$$\frac{\partial \sigma}{\partial n}(\mathbf{x}) = \lim_{h \to 0} \frac{\sigma(\mathbf{x} + h\mathbf{n})}{h}, \quad \mathbf{x} \in \Gamma. \tag{4.24}$$

The normal derivative to the adjoint variable σ is obtained by evaluating the solution σ at an interior point $\mathbf{x} + h\mathbf{n} \in \Omega$ close to the boundary and dividing by the distance h from the boundary. Equations (4.22a)-(4.22b) is a Poisson problem with non-homogeneous right hand side, the method of finding a solution to such a problem with BIE is not trivial when a source term is present. The IBEM approach developed in Chapter (3) can no longer be directly used. However, if the Green's function is known for Ω the solution can be found analytically. Consider a solution on the form

$$\sigma(\mathbf{x}) = \int_{\Omega} G(\mathbf{x}, \mathbf{y}) f(\mathbf{y}) \, d\mathbf{y}, \tag{4.25}$$

and let $G(\mathbf{x}, \mathbf{y})$ be the free space solution to Laplace's equation, then (4.25) is a particular solution to (4.22a). This solution does not necessarily satisfy the homogeneous boundary condition (4.22b). Instead, consider a modified Green's function $G_\Omega(\mathbf{x}, \mathbf{y})$ that does satisfy the boundary condition on Γ in addition to being a solution to (4.22a). To do this, define a new function v_Ω that satisfies

$$\Delta v_\Omega(\mathbf{x}, \mathbf{y}) = 0, \qquad \mathbf{x} \in \Omega \tag{4.26a}$$

$$v_\Omega(\mathbf{x}, \mathbf{y}) = G(\mathbf{x}, \mathbf{y}), \quad \mathbf{x} \in \Gamma \ . \tag{4.26b}$$

With $G_\Omega(\mathbf{x}, \mathbf{y}) := G(\mathbf{x}, \mathbf{y}) - v_\Omega(\mathbf{x}, \mathbf{y})$,

$$\sigma(\mathbf{x}) = \int_{\Omega} G_\Omega(\mathbf{x}, \mathbf{y}) f(\mathbf{y}) \, d\mathbf{y}, \tag{4.27}$$

solves the boundary values problem (4.22a)-(4.22b). For arbitrary bounded domains, finding a Green's functions that satisfy (4.26a)-(4.26b) is not easy. For well known simple domains such as the disc there is a method known as the *method of images* [22] to construct the Green's function. Let Ω be the unit disc with radius $R = 1$, the Green's function in polar coordinates is [22]

$$G_\Omega(r, \theta, r_0, \theta_0) = \frac{1}{4\pi} \log \left(\frac{r^2 + r_0^2 - 2rr_0 cos(\theta - \theta_0)}{r^2 r_0^2 + 1 - 2rr_0 cos(\theta - \theta_0)} \right), \tag{4.28}$$

substituting (4.28) into (4.27) finally solves the boundary value problem. In (4.22a), and considering the adjoint problem (2.19a)-(2.19b), f is known as $f = u - u_{target}$. For the state variable u we consider the test problem (A.0.1) with a constant $C = 1$ on Γ, u is solved for with the interior IBEM Laplace solver. For u_{target}, by (2.5), we here consider an exterior point z_p far away from the boundary such that $u_{target} = 0$. The solution to the adjoint variable σ is obtained from (4.27). Again, two different methods are here considered for numerical evalua-

tion of the integral in (4.27), the first one is based on evaluating the integrand at the center of the disc and then multiplying by the area of the disc [1] and the other by Gauss-Legendre quadrature for double integrals in polar coordinates with the same number of quadrature points, coordinates and weights as for the quadrature in Section (4.0.2).

When evaluating the Green's function at the center of the disc, $r_0 = 0$, the Green's function simplifies to

$$G_\Omega(r, \theta, 0, \theta_0) = \frac{1}{4\pi} \log\left(r^2\right), \tag{4.29}$$

let $h = 1 - r$ denote the distance from the boundary at an interior point $re^{i\theta} \in \Omega$, then

$$\frac{\sigma(r,\theta)}{1-r} = \frac{\pi \frac{1}{4\pi} \log(r^2) \left[u(0,\phi) - u_{target}(0)\right]}{1-r}, \tag{4.30}$$

is an estimate for the normal derivative in (4.24) employing the center point method. When r tends towards $R = 1$ it is expected that the normal derivative converges to its true value. For the unit disc, the analytical normal derivative to the test problem (A.0.3) is then $\frac{1}{2}$ when $B_0 = 1$. In Figure (4.8) the solution to (4.30) is plotted.

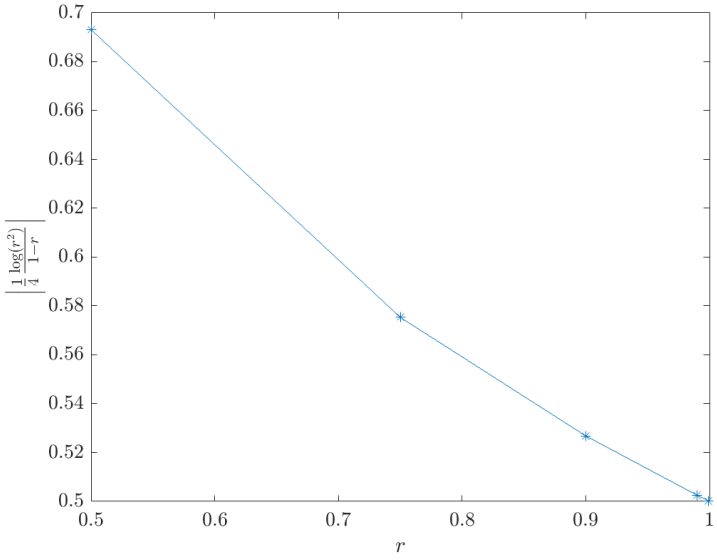

Figure 4.8: Computing the analytical expression $\left|\frac{\sigma(r,\theta)}{1-r}\right|$ in (4.30) with $u(0,\phi) = 1$ and $u_{target} = 0$.

Clearly, the results in Figure (4.8) show that the normal derivative is estimated correctly since it converges to the true value of $\left|\frac{\partial\sigma(r,\theta)}{\partial n}\right| = \frac{1}{2}$ according to the test problem (A.0.3). For Gauss-Legendre quadrature, the result for

$$\left|\frac{\partial\sigma}{\partial n}\right| \approx \left|\frac{\sigma(r,\theta)}{1-r}\right|, \tag{4.31}$$

[1] Here this is referred to as *the center point method*.

is presented in Figure (4.9) where $\sigma(r,\theta)$ is computed by numerically integrating (4.27) at a fixed distance $h = 1-r$ close to the boundary by Gauss-Legendre quadrature with $f(\mathbf{y}) = 1$ and with G_Ω from (4.28). Again, we consider the test problem (A.0.3) and the analytic normal derivative $\left|\frac{\partial\sigma(r,\theta)}{\partial n}\right| = \frac{1}{2}$ is here used as a reference solution.

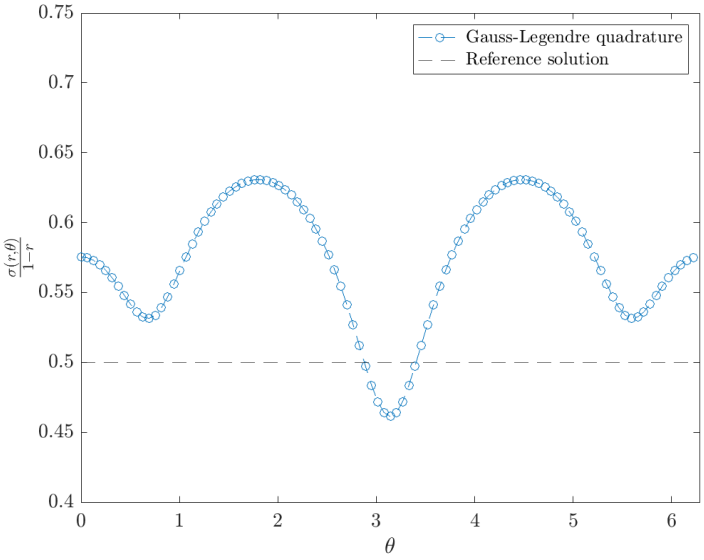

Figure 4.9: Computing (4.31) pointwise over Γ with Gauss-Legendre quadrature for $\sigma(r,\theta)$ at a fixed distance $h = 1-r = 0.3$ from the boundary.

The results in Figure (4.9) does not agree with the reference solution when $h = 1-r = 0.3$. The approximation to the normal derivative seems to oscillate around a value of between ≈ 0.45 and ≈ 0.65. We know analytically the true value to be $\frac{1}{2}$ for all θ.

κ-test results for a constant perturbation ϕ'

The distance $h = 0.3$ from the boundary Γ is not close to 0. κ-tests has been performed to explain the reason for h not being smaller. In the following κ-tests, the state variable u is solved for with the interior IBEM Laplace solver utilizing the center-point method, as well as with and without the two-point linear interpolation previously discussed in section (3.2.3). The directional normal derivative (4.31) is computed with Gauss-Legendre quadrature where $f = u - u_{target}$ with $u_{target} = 0$. We consider cases where

- the number of discretization points N is fixed and the distance h from the boundary is varied
- the number of discretization points N are varied and the distance h from the boundary is fixed.

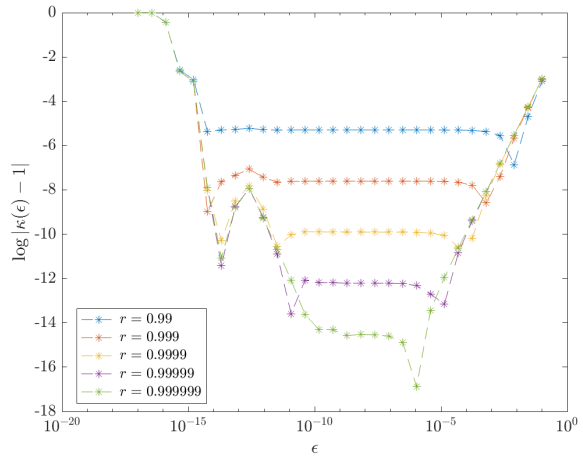

(a) Fixed number of discretization points $N = 100$ on the boundary and varying distance $h = 1 - r$ from boundary with the center point method.

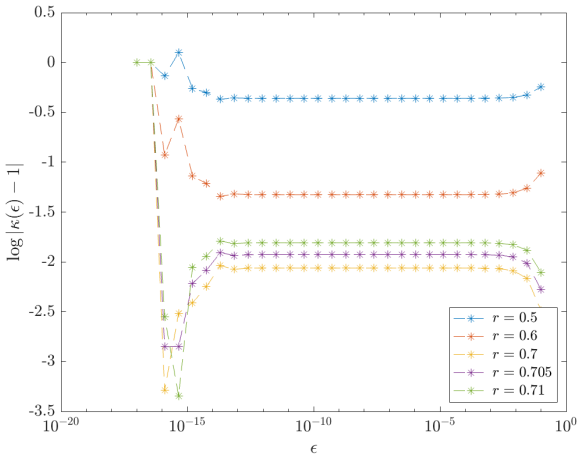

(b) Fixed number of discretization points $N = 100$ on the boundary and varying the distance $h = 1-r$ from the boundary with the interior Laplace solver.

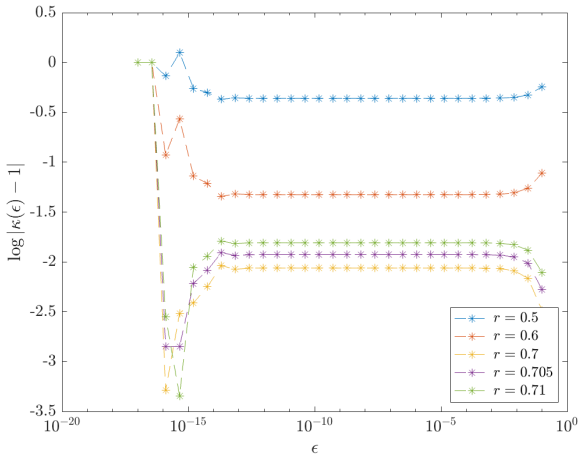

(c) Fixed number of discretization points $N = 100$ on the boundary and varying the distance $h = 1-r$ from the boundary utilizing interpolation with the interior Laplace solver.

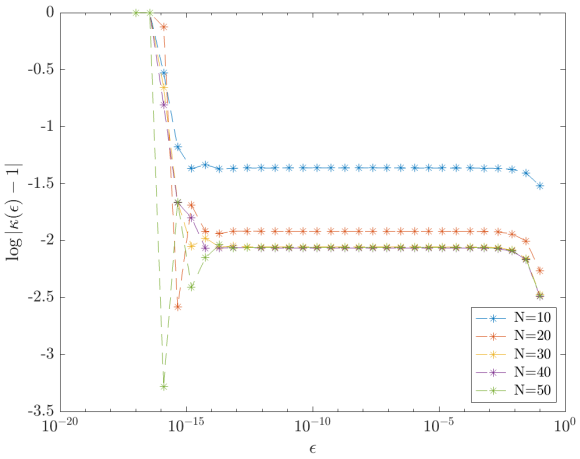

(d) Fixed distance $h = 1 - r = 0.3$ from boundary and varying number of discretization points N on the circle with the interior Laplace solver.

Figure 4.10: κ-test results for directional derivative approach with constant Dirichlet data $\phi(z) = 1$ and a constant perturbation $\phi'(z) = 1.01$. State variable u is computed by solving Laplace's equation (2.11a)-(2.11b) with the interior IBEM solver developed in section (3.2). $\phi(z)$ denotes the Dirichlet data in (2.11b) and $\phi'(z)$ denotes the perturbation in (2.14b). Here, we consider a point z_p in (2.5) & (2.4) far away from the boundary such that $u_{target} = 0$.

As seen in figure (4.10a) it is noted that as the the distance from the boundary decrease, the error does also decrease which is expected behaviour. When the integral for the normal derivative is estimated by quadrature, it is noted in Figure (4.10b) that the error decrease when approaching the boundary. However, at $h < 1 - r = 0.3$ the error increase again when approaching the boundary. For $N = 100$ discretization points, we know from section (3.2.3) that the IBEM has accuracy close to machine epsilon, thus this increase in error is likely due to the fact that the Green's function is estimated inaccurately close to the boundary. Moreover, the two point linear interpolation from section (3.2.3) has been utilized and the results in Figure (4.10c) are indistinguishable from the results obtained

without any interpolation. This further suggests that the error increase due to the evaluation of the Green's function and not due to errors when evaluating $f = u - u_{target}$ in (4.27). Thus, without any explicit treatment for integrating Green's type integrals there is a bound on how close to the boundary we can get with this method before the results are no longer satisfactory. In Figure (4.10d) we see that the error decrease as the number of discretization points increase up to $N = 50$ for $r = 1 - h = 0.3$, these results are in line with the results obtained in Figure (3.1a), with this method, the best results are obtained with $N = 50$ and $h = 0.7$.

4.0.4 Section (3.3) revisited: Boundary Flux by Direct BEM for Poisson's equation

Consider an interior Dirichlet problem with a source term f defined on Ω where the desired information is the unknown boundary flux in the normal direction to the boundary. The Poisson equation reads

$$\begin{aligned} \Delta U &= f, \qquad \text{in } \Omega, \\ U &= g_d, \qquad \text{on } \Gamma \ . \end{aligned}$$

As previously discussed in Chapter (3) on BEMs, one of the main advantages of BEMs is that the problem can be expressed on the boundary only and thus there need not be any internal discretization of the domain. With a source term present there is still an integral over the entire domain that has to be carried out [12]. Several methods has been proposed on how to deal with this problem. These methods typically involves solving for a particular solution and fitting this to the boundary data for the corresponding homogeneous problem, this is known as homogenization. This is similar to the method as outlined for constructing the Green's function for solving Poisson's equation analytically. This requires an efficient numerical method for solving for the particular solution and has been shown that be of considerable difficulty. However, if the source term is harmonic, it turns out it is indeed possible to rewrite the problem in terms of boundary integrals only, circumventing the problem of having to discretize the interior of the domain [12]. Moreover, here we only consider homogeneous Dirichlet data $g_d = 0$ as this is what we have for the adjoint Poisson problem (2.19a)-(2.19b). In many problems of this type, the Dirichlet data on Γ is known and the boundary flux $\frac{\partial U}{\partial n}$ is unknown and desired information. Consider the Dirichlet problem augmented with $\Delta f = 0$

$$\Delta U = f, \qquad \text{in } \Omega, \tag{4.33a}$$

$$U = g_d = 0, \qquad \text{on } \Gamma, \tag{4.33b}$$

$$\Delta f = 0, \qquad \text{in } \Omega \ . \tag{4.33c}$$

Instead of using an indirect approach such as the IBEM it is more suitable to now consider the DBEM. Following the works of [12], for a 2D Poisson problem, this results in a boundary integral equation formulated as

$$\int_\Gamma \frac{1}{r}\frac{\partial U}{\partial n}\, dl = \int_\Gamma \left(f\frac{\partial h}{\partial n} - h\frac{\partial f}{\partial n} \right)\, dl, \tag{4.34}$$

where $h = \frac{1}{4}r^2(\log(r) - 1)$ is the fundamental solution to the biharmonic equation $\Delta^2 h = 0$ and $r = |x - x_0|$. The idea is to obtain the boundary flux of the source term $\frac{\partial f}{\partial n}$ by formulating Laplace's equation as a DBEM as outlined in section (3.3). With h, $\frac{\partial h}{\partial n}$ and f given as well as an approximation for $\frac{\partial f}{\partial n}$ available one then solves for the boundary flux $\frac{\partial U}{\partial n}$ using (4.34). Now, since the source term $f = u - u_{target}$ in the adjoint equations (2.19a)-(2.19b) is a superposition of two primal solutions (that by definition are solutions to Laplace's equation) the normal derivative $\frac{\partial \sigma}{\partial n}$ of the adjoint variable σ is found by solving (4.33a)-(4.33c) with $U = \sigma$ and $f = u - u_{target}$. Since the DBEM has shown to give erroneous results (possibly due to degenerate scale issues) for Laplace's equation it has not been possible to continue with the Poisson implementation. However, this is included here since this seems to be the most promising method of solving for the adjoint boundary flux with a boundary element method.

Chapter 5

Reconstruction of Dirichlet Data on the Boundary

5.1 Outline of Shape Optimization

This section is devoted to using the optimization techniques developed in Chapter (2) for a prototype for shape optimization. The idea for shape optimization is to formulate the optimization problem with the help of shape derivatives [1] and to reconstruct the shape by first solving the primal problem and then the corresponding adjoint problem to determine the Riesz representer. The idea is to have a shape-vector θ and reconstruct θ to converge to an optimal shape given a target solution. However, in practise the target state $u_{target} = u(\widehat{\phi})$ that has been considered throughout this thesis is unknown and we should in practical applications consider an inverse problem. The optimal control variable $\widehat{\phi}$ as defined by (2.4) has been employed here for the purpose of verifying the numerical solvers. Instead of shape derivatives we will here consider a prototype that reconstruct initial Dirichlet data on the boundary.

5.2 Reconstruction of Dirichlet Data on the boundary Γ

The end result of this thesis work consist of an implementation of the Polak-Ribiere method for reconstruction of the Dirichlet data on Γ where the primal Laplace's equation with Dirichlet data on Γ is solved with the IBEM with the interior IBEM Laplace solver (which is appended in Appendix (B)). The adjoint problem is solved on the unit disc to machine accuracy based on quadrature identities for the unit disc. The adjoint solver works for the unit disc, further work has to be done to extend this to other geometries.

[1] Shape derivatives are briefly discussed in Section (6.2.2).

5.2.1 Reconstruction of constant initial Dirichlet data

For this model problem, a constant step length τ is used instead of (2.7), where line search is used. The initial guess (2.1) for the Dirichlet data is set to a constant $\phi^{(0)}(\theta) = \phi^{(0)}$ on Γ where θ is some angle on the boundary. The target solution u_{target} is computed with the interior IBEM Laplace solver as a function of the target Dirichlet data $\widehat{\phi}(\theta) = \widehat{\phi}$ such that $u_{target} = u(\widehat{\phi})$. The integrals in the β-term (2.8b) is computed by the 2^{nd} quadrature identity (4.5b) and the functional $\mathcal{J}$ is computed by the 1^{st} quadrature identity (4.5a). An absolute value for the functional $\mathcal{J}$ is set as a tolerance condition and the functional is for this case expected to tend to zero when minimized. The Riesz representer is computed by the directional derivative approach with the center point method, i.e. by equation (4.30). The full MATLAB/Octave implementation is found in Appendix (C). With this method, the functional $\mathcal{J}$ is successfully minimized on the unit disc when the Dirichlet data ϕ is reconstructed to the target $\widehat{\phi}$.

5.2.2 Non-Linear Conjugate-Gradients (Polak-Ribiere) Results

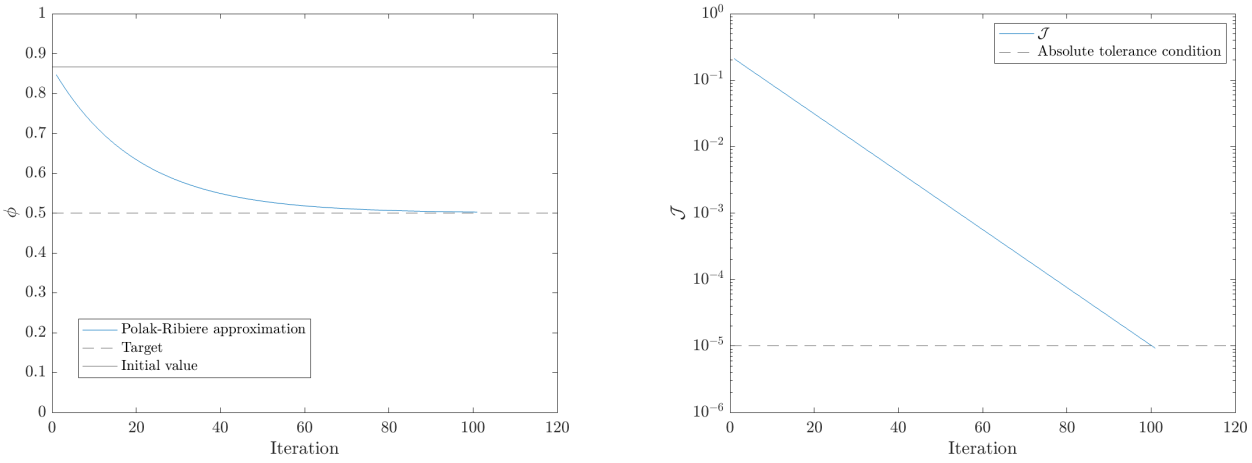

(a) ϕ (b) $\mathcal{J}$

Figure 5.1: Polak-Ribiere Results.

The parameters used are presented in Table (5.1) and the method converged in 101 iterations.

τ	max_{iter}	tol	$\phi^{(0)}$	$\widehat{\phi}$
0.1	200	10^{-5}	$\sin(\pi/3)$	0.5

Table 5.1: Parameters used for Polak-Ribiere implementation.

Chapter 6

Main Results, Conclusions & Future work

6.1 Results and Conclusions

The methods outlined in this thesis presents a prototype that acts as a foundation for building towards the shape optimization problems discussed in Chapter (1). The numerical solvers does not in fact optimize the shape, rather the Dirichlet data on the boundary. For the sake of generality, the continuous adjoint formulation from Chapter (2) has been employed, and in the same notion the non-linear Polak-Ribiere method has been implemented, albeit not necessary for the linear problems considered in this thesis.

In Chapter (3) it is concluded that the IBEM works very well for interior Dirichlet problems for Laplace's equation but there might be degenerate scale issues for the corresponding exterior Dirichlet problem. For the sake of robustness when moving on to more complicated domains it is thus recommended to make use of the Kelvin transformation if one seeks to further develop a solver for exterior flow problems.

In Chapter (4) it has become evident that solving Poisson's equation for the boundary flux with BEMs is difficult when the domain is anything other than the circle. In Section (3.4) it has been discussed that there are some erroneous results when computing the analytical integrations for solving Laplace's or Poisson's equation by the DBEM as there might be an issue of degenerate scale by using this method. Despite of these drawbacks, the DBEM is a good candidate for researchers looking to build upon the methods presented in this thesis. This is due to the fact that the DBEM for Poisson's equation is directly applicable to Laplace's equation, whereas the indirect approach is only applicable for Laplace's equation. Another suggestion is to use the IBEM solver for the primal

problem in combination with a DBEM solver for the adjoint problem. In general, these results shows that the choice of developing these methods with the continuous adjoint formulation was a good one since there is much freedom in choosing the discretization method of the primal and adjoint problems.

6.2 Future work

6.2.1 Normal derivative

The Green's function and its Poisson Kernel presented in Chapter (4) are analytic but suffer from erroneous results when attempting to compute the normal derivative. Even though the integrands are analytic they suffer from cancellation errors when evaluating small values on computers with 16 digit arithmetic. Trefethen and Weideman suggests a possible remedy for this problem on the unit disc that is based on Cauchy integrals in the complex plane in order to deal with removable singularities [35].

6.2.2 Shape derivatives

Now we are in a position to revisit the conceptual Figure (1.1) and to briefly introduce the notion of shape derivatives and Hadamard's Boundary variation method. The functional $\mathcal{J}$ is now instead defined as

$$\mathcal{J}(\Omega_\theta) = \mathcal{J}(\Omega) + \mathcal{J}'(\Omega)(\theta) + \mathcal{O}(\theta), \tag{6.1}$$

where the linear mapping $\theta \to \mathcal{J}'(\Omega)(\theta)$ is the shape derivative of the functional $\mathcal{J}$ at Ω [5]. Hadamard's boundary variation method suggests a perturbation of a reference domain Ω, where Ω is a Lipschitz domain [5]

$$\Omega \to \Omega_\theta := (Id + \theta)\Omega \ . \tag{6.2}$$

The idea is to make use of the optimization framework developed for this thesis, where the perturbation vector θ is used to minimize $\mathcal{J}$ with respect to its shape derivatives. In [5], Bonnetier and Dapogny take such an approach in an adjoint setting for Laplace's equation similar to what has been done in this thesis work, however, not utilizing BEMs. Their work is a good starting point if one seeks to continue the work developed for this thesis.

Appendices

Appendix A

Analytic solutions to test problems.

When dealing with complex geometries, to find analytical solutions is in general not a trivial task and one has to resort to numerical approximations. For some simple and symmetric geometries, such as the circle, there exist analytical solutions to Laplace's equation and Poisson's equation. The problems presented here are subject to Dirichlet boundary conditions where the desired solution is either the solution at a point inside an interior domain or the boundary flux in the direction normal to the boundary.

A.0.1 Laplace's equation with constant Dirichlet boundary condition.

Consider the interior Dirichlet boundary value problem (Laplace's equation) on a circle with radius R with constant Dirichlet boundary condition

$$\Delta u(r,\theta) = 0, \quad (r,\theta) \in \Omega, \tag{A.1a}$$

$$u(r = R,\theta) = C, \quad (r,\theta) \in \Gamma\ . \tag{A.1b}$$

The strong maximum principle for harmonic functions states that a non-constant harmonic function cannot attain a maximum or minimum at an interior point of its domain [11]. By the strong maximum principle for harmonic functions, if there exist a solution u to (A.1a)-(A.1b) then u is the unique solution to the boundary value problem [11]. Thus, $u = C$ is a unique solution to (A.1a)-(A.1b) since it satisfies the boundary condition (A.1b) and $\Delta u = \Delta(C) = 0$. A consequence of the strong maximum principle for harmonic functions is that in a bounded domain, the values of a harmonic function is bounded by the maximum and minimum values on the boundary [11]. With constant boundary data on Γ, asserting that u is non-constant results in a contradiction by the strong maximum principle for harmonic functions. Thus, with constant boundary data, the solution u is constant in the domain.

A.0.2 Laplace's equation with non-constant Dirichlet boundary condition

Consider the Dirichlet boundary value problem (Laplace's equation) on the unit circle

$$\Delta u(r,\theta) = 0, \qquad (r,\theta) \in \Omega, \tag{A.2a}$$

$$u(r,\theta) = u(\theta) = f(\theta) = 1 + A\sin(\theta), \quad (r,\theta) \in \Gamma\ . \tag{A.2b}$$

On the unit circle, $r = 1$, the solution to (A.2a)-(A.2b) is $u(r,\theta) = 1 + Ar\sin(\theta)$. This clearly satisfies (A.2b). It is a solution to (A.2a) since

$$\Delta u(r,\theta) = u(r,\theta)_{rr} + \frac{1}{r}u(r,\theta)_r + \frac{1}{r^2}u_{\theta\theta}\ ,$$

$$(1 + Ar\sin(\theta))_{rr} + \frac{1}{r}(1 + Ar\sin(\theta))_r + \frac{1}{r^2}(1 + Arsin(\theta))_{\theta\theta} = \frac{A}{r}\sin(\theta) + \frac{1}{r^2}(-Ar\sin(\theta)) = 0\ .$$

A.0.3 Poisson's equation with homogeneous Dirichlet boundary condition and constant source term

Consider the interior Dirichlet boundary value problem (Poisson's equation) on circle with radius R with homogeneous boundary condition

$$\Delta\sigma(r,\theta) = u(r,\theta) = B_0, \quad (r,\theta) \in \Omega, \tag{A.3a}$$

$$\sigma(r = R,\theta) = 0, \qquad (r,\theta) \in \Gamma\ . \tag{A.3b}$$

In (A.3a)-(A.3b), $u(r,\theta)$ is assumed to be the solution to Laplace's equation from test problem (A.0.1). The solution to (A.3a)-(A.3b) is radially symmetric and is obtained as [33]

$$\sigma(r) = \frac{B_0}{4}(r^2 - R^2), \tag{A.4}$$

where $0 \le r \le R$. The boundary flux is obtained as

$$\frac{\partial\sigma}{\partial n} = \frac{\partial\sigma}{\partial r}\bigg|_{r=R} = \frac{B_0 R}{2}, \tag{A.5}$$

since the solution is radially symmetric it follows that the boundary flux is constant on the boundary.

Appendix B

Primal IBEM Laplace Solver

B.1 Main program file

The following file includes the interior (IBEM) Laplace solver that also performs a κ-test, the center point method is used for computing the functional as well as the normal derivative.

```
clear all, close all, clc, format long
%profile on
N_t_vec = [20:20:100];
nt = 0;
for N_t = N_t_vec
    nt = nt + 1;
    R = 1; %Radius of circle
    rmin = 0; rmax = R; %integration limits
    tmin = 0; tmax = 2*pi; %integration limits
    phi = 1; phi_prim = 1.01;
    h_t = 2*pi/(N_t); t_vec = [0:h_t:2*pi-h_t]; %step length and theta-
        discretization
    z = R*exp(1i*t_vec); z_prim = 1i*z; z_prim_prim = 1i*z_prim; %
        parametrization
    K = BIE_kernel(N_t, R, z, z_prim, z_prim_prim, h_t, t_vec); I = eye(N_t);
        mat = ((1/2)*I+K); %compute integral kernel, identity matrix and compose
         system
    %mu_phi = gmres(mat, phi.*ones(length(t_vec'), 1));
    phi_vec = phi.*ones(length(t_vec), 1); %Dirichlet data
```

```
%phi_vec = randn(length(t_vec), 1);
phi_prim_vec = (1.2-0.8).*rand(length(t_vec),1) + 0.8; %randomize a
    perturbation vector over the boundary
%phi_vec = phi.*ones(length(t_vec), 1); %phi_prim_vec =
%phi_prim.*ones(length(t_vec), 1); %comment out if testing for constant
%perturbation data instead
mu_phi = gmres(mat, phi_vec); mu_phi_prim = gmres(mat, phi_prim_vec); %
    boundary density for Dirichlet data and for perturbation data
%R = 1 lies on unit circle, R > 1 lies outside of unit circle
%R_target = 1.0000000000001; %choose target point close to boundary
R_target = 1000000000; %choose target point far away from boundary
theta_target = (2*pi-0)*rand(1,1); %randomize angular direction for target
    point
mu_target = gmres(mat, (imag ( (exp(1i.*t_vec').^2)./(exp(1i.*t_vec')-
    R_target*exp(1i.*theta_target)) ))); %compute boundary density for
    target solution
z_0 = 0; %set interior point to center point to evaluate with center point
    method
U_phi = 0; U_phi_prim = 0; U_d = 0; %initialize values
%Loop over number of points along theta-direction on the boundary
for j = 1:N_t
    y(j) = z_prim(j)./(z(j)-z_0);
    y = imag(y);
    U_phi = U_phi + mu_phi(j)*y(j); U_phi_prim = U_phi_prim + mu_phi_prim(j
        )*y(j); U_d = U_d + mu_target(j)*y(j);
end
scale = (h_t/(2*pi)); U_d_0 = scale*U_d; U_phi_0 = scale*U_phi;
    U_phi_prim_0 = scale*U_phi_prim;
U_phi = scale*U_phi; U_phi_prim = scale*U_phi_prim; U_d = scale*0;
f_z0=( U_phi-U_d ).^2;
J_phi_center =0.5*pi*R^2*f_z0; %Compute functional with center point method
%For kappa-testing
epsilon_vec = logspace(-17, -1, 30); e = 0;
for epsilon = epsilon_vec
```

```
        e = e + 1;
        f_z0_eps =( U_phi_0+epsilon*U_phi_prim_0-U_d_0 ).^2;
        J_phi_epsilon_center =0.5*pi*R^2*f_z0_eps;
        Gateaux_derivative(e) = (1/epsilon)*(J_phi_epsilon_center-J_phi_center)
            ;
    end
    pointwise_normal_derivative = 0.5*(U_phi_0-U_d_0); %compute normal
        derivative with center point method
    %Integrate adjoint solution multiplied by phi_prim over boundary theta=[0,
        2pi]
    J_prim_adjoint = pointwise_normal_derivative*2*pi*R*mean(phi_prim_vec);
    kappa(nt, :) = Gateaux_derivative./J_prim_adjoint; %store kappa values
end
figure
[mm, nn] = size(kappa);
for m = 1:mm
   semilogx(epsilon_vec, log10(abs(kappa(m, :)-1)), '--*'), hold on
end
for iN = 1:length(N_t_vec)
  legendCell{iN} = num2str(N_t_vec(iN),'N=%g');
end
legend(legendCell, 'Location', 'southeast')
hold off
ax = gca;
ax.FontSize = 14;
title("\kappa-test")
xlabel('\epsilon')
ylabel('log|\kappa(\epsilon)-1|')
%profile viewer
```

B.2 Supporting program files

```
function K = BIE_kernel(N, R, z, z_prim, z_prim_prim, h, t_vec)
    % i, j = 0, 1, ..., N-1
    %h = 2*pi/N; t_vec = [0:h:2*pi-h];
    %parametrization for a circle
    %z = R*exp(1i*t_vec); z_prim = 1i*z; z_prim_prim = 1i*z_prim;
    %Integral kernel
    %K_ij=(h/2*pi)*imag(z_jprim/(z_j-z_i));
    K = zeros(N);
    for i = 1:N
        for j = 1:N
            if (i == j)
                K(i,i)= imag(z_prim_prim(i)/(2*z_prim(i)));
            else
                K(i, j)=imag( z_prim(j)/(z(j)-z(i)));
            end
        end
    end
    K = (h/(2*pi))*K;
end
```

Appendix C

Polak-Ribiere Implementation

C.1 Main program file

```
%%
clear all
clc
close all
%%
N_p = 50; %N_p = number of discretization points on the boundary
theta_vec = [0:2*pi/N_p:2*pi-2*pi/N_p];
phi0 = sin(pi/3)*ones(N_p, 1); phi = phi0; d_tau = 0.1; %Initial guess for
    Dirichlet data and step-length
global phi_target; phi_target = 0.5*ones(N_p, 1);  %phi_target = cos(theta_vec)
    ';
tmin = 0; tmax = 2*pi;
maxiter = 10000; %terminate after maxiter if tolerance condition has not been
    reached
i = 1;
tol = 1e-5; %tolerance condition
%% Do first 2 iterations to store values in memory for tolerance condition
% 1st iteration
[J_phi, gradJ, U_phi_center, U_target_center] = solve_J_and_grad_J_PR(phi);
J_phi_vec(i) = J_phi;
gradJ_phi_p_vec(i) = gradJ;
```

```
p = -gradJ; %p_0 = -gradJ %p = (conjugate) descent direction
phi=phi+d_tau*p;
%phi_vec(i) = phi;
i = i + 1;
% 2nd iteration
[J_phi, gradJ, ~, ~] = solve_J_and_grad_J_PR(phi);
J_phi_vec(i) = J_phi;
gradJ_vec(i) = gradJ;
%compute momentum term beta
[~, gradJ_point_old, ~, ~] = solve_J_and_grad_J_PR(phi0); %compute pointwise
    gradient on Gamma for old phi (on the disc normal derivative is constant for
     all theta)
[~, gradJ_point, ~, ~] = solve_J_and_grad_J_PR_2(phi); %compute pointwise
    gradient on Gamma for current phi (on the disc normal derivative is constant
     for all theta)
momentum_beta = gradJ_point*(gradJ_point-gradJ_point_old)/(gradJ_point_old^2);
p = -gradJ + momentum_beta*p; %(conjugate) descent direction
phi_old = phi;
phi=phi+d_tau*p;
%phi_vec(i) = phi;

%% Main optimization loop
err(i) = abs(J_phi_vec(i) - J_phi_vec(i-1))/abs(J_phi_vec(i-1));
while ( abs(J_phi_vec(i))  > tol && (i <= maxiter) )
        i = i + 1;
        [J_phi, gradJ, ~, ~] = solve_J_and_grad_J_PR(phi); %compute (pointwise
            gradient at theta_test=t) and functional at theta_test;
        %and store the results for plotting and for checking error condition
        J_phi_vec(i) = J_phi; gradJ_vec(i) = gradJ;
        %compute momentum term beta
        [~, gradJ_point_old, ~, ~] = solve_J_and_grad_J_PR(phi_old); %compute
            pointwise gradient on Gamma for old phi
        [~, gradJ_point, ~, ~] = solve_J_and_grad_J_PR(phi); %compute pointwise
             gradient on Gamma for current phi
```

```
        momentum_beta = 2*pi*gradJ_point*(gradJ_point-gradJ_point_old)/(
            gradJ_point_old^2);

        p = -gradJ + momentum_beta*p; %p = (conjugate) descent direction
        phi_old = phi;
        phi = phi + d_tau*p; %phi_vec(i) = phi; %update phi (at theta point on
            boundary) and store new phi for plotting

        rel_err = abs(J_phi_vec(i) - J_phi_vec(i-1) ) / abs(J_phi_vec(i-1));
            err(i) = rel_err; %compute error for convergence analysis
end
```

C.2 Supporting program files

```
function [J_phi, gradJ_phi_p, U_phi, U_d] = solve_J_and_grad_J_PR(phi)
    global phi_target;
    N_t = 50; %Number of discretization points on the boundary
    R = 1; %Radius of circle/disc
    rmin = 0; rmax = R; %integration limits
    tmin = 0; tmax = 2*pi; %integration limits
    h_t = 2*pi/N_t; t_vec = [0:h_t:2*pi-h_t]; %discretization & parametrization
    %Interior (IBEM) Laplace solver
    z = R*exp(1i*t_vec); z_prim = 1i*z; z_prim_prim = 1i*z_prim; %
        parametrization
    K = BIE_kernel(N_t, R, z, z_prim, z_prim_prim, h_t, t_vec); I = eye(N_t);
        mat = ((1/2)*I+K); %matrices
    mu_phi = gmres(mat, phi); %primal boundary density
    mu_target = gmres(mat, phi_target); %target boundary density
    %let z_0 be the interior point corresponding to r=r_0, theta_0, z_0 = 0;
    U_phi = 0; U_d = 0; %initialize variables
    %Loop over N_t number of points along theta-direction on the boundary
    for j = 1:N_t
        y(j) = z_prim(j)./(z(j));
        y = imag(y);
```

```
        U_phi = U_phi + mu_phi(j)*y(j);
        U_d = U_d + mu_target(j)*y(j);
    end
    scale = (h_t/(2*pi)); U_phi = scale*U_phi; U_d = scale*U_d; %scaling
    J_phi =0.5*pi*R^2*( U_phi-U_d ).^2; %Compute functional (J_phi) with center
        -point method
    %Compute adjoint solution
    h = 0.05; %distance from boundary
    r_p = R-h; %radial distance to interior point for computing normal
        derivative with directional derivative approach
    theta_0 = pi/2; %can be anything between 0 and 2*pi due to radial symmetry
        when evaluated at r_0=0
    r_0 = 0;
    %Evaluates Riesz representer by the directional derivative approach using
        the
    % center point method for (primal) state & target_state
    % and analytic expression for Green's function for the unit disc
    gradJ_phi_p = abs(0.25*log(r_p^2)*(U_phi-U_d)/h);
end
```

Bibliography

[1] Lars V. Ahlfors. *COMPLEX ANALYSIS. An Introduction to the Theory of Analytic Functions of One Complex Variable*. INTERNATIONAL SERIES IN PURE AND APPLIED MATHEMATICS. McGraw-Hill, Inc, 1979. ISBN: 0-07-000657-1.

[2] Atkinson. *The Numerical Solution of Integral Equations of the Second Kind*. Cambridge Monographs on Applied and Computational Mathematics. Cambridge University Press, 1997. ISBN: 0-521-58391-8.

[3] Daryoush Behmardi and encyeh Dehghan Nayeri. "Introduction of Fréchet and Gâteaux Derivative". In: *Applied Mathematical Sciences* 2.20 (2008), pp. 975–980. URL: http://www.m-hikari.com/ams/ams-password-2008/ams-password17-20-2008/behmardiAMS17-20-2008.pdf.

[4] Steven R. Bell, Bjorn Gustafsson, and Zachary A. Sylvan. *Szego coordinates, quadrature domains, and double quadrature domains*. 2010. arXiv: 1003.2195 [math.CV].

[5] Éric Bonnetier and Charles Dapogny. *An introduction to shape and topology optimization*. Last accessed 23 October 2023. 2020. URL: https://membres-ljk.imag.fr/Charles.Dapogny/coursoptim/slides/PartIII_Hadamard_Method.pdf.

[6] J. Brebbia C.A. Dominguez. *Boundary Elements: An Introductory Course*. McGraw Hill, 1992.

[7] J.T. Chen et al. "An alternative method for degenerate scale problems in boundary element methods for the two-dimensional Laplace equation". In: *Engineering Analysis with Boundary Elements* 26.7 (2002), pp. 559–569. ISSN: 0955-7997. DOI: https://doi.org/10.1016/S0955-7997(02)00024-3. URL: https://www.sciencedirect.com/science/article/pii/S0955799702000243.

[8] Jeng-Tzong Chen et al. "A self-regularized approach for rank-deficient systems in the BEM of 2D Laplace problems". In: *Inverse Problems in Science and Engineering* 25.1 (2017), pp. 89–113. DOI: 10.1080/17415977.2016.1138948. eprint: https://doi.org/10.1080/17415977.2016.1138948. URL: https://doi.org/10.1080/17415977.2016.1138948.

[9] Jeng-Tzong Chen et al. "Revisit of a degenerate scale: A semi-circular disc". In: *Journal of Computational and Applied Mathematics* 283 (2015), pp. 182–200. ISSN: 0377-0427. DOI: https://doi.org/10.1016/j.cam.2015.01.011. URL: https://www.sciencedirect.com/science/article/pii/S0377042715000230.

[10] Ansys Innovation Courses. *Simple Approximations of Fluid Flows*. Last accessed 23 October 2023. 2020. URL: https://courses.ansys.com/index.php/courses/simple-approximations-of-fluid-flows/.

[11] Lawrence C. Evans. *Partial Differential Equations*. Graduate Studies in Mathematics. American Mathematical Society, 1997.

[12] Graeme Fairweather et al. "On the numerical solution of two-dimensional potential problems by an improved boundary integral equation method". In: *Journal of Computational Physics* 31.1 (1979), pp. 96–112. ISSN: 0021-9991. DOI: https://doi.org/10.1016/0021-9991(79)90064-0. URL: https://www.sciencedirect.com/science/article/pii/0021999179900640.

[13] M. Fratantonio and J.J. Rencis. "Exact boundary element integrations for two-dimensional Laplace equation". In: *Engineering Analysis with Boundary Elements* 24.4 (2000), pp. 325–342. ISSN: 0955-7997. DOI: https://doi.org/10.1016/S0955-7997(00)00005-9. URL: https://www.sciencedirect.com/science/article/pii/S0955799700000059.

[14] Parviz Ghadimi, Abbas Dashtimanesh, and Hossein Hosseinzadeh. "Solution of Poisson's equation by analytical boundary element integration". In: *Applied Mathematics and Computation* 217.1 (2010), pp. 152–163. ISSN: 0096-3003. DOI: https://doi.org/10.1016/j.amc.2010.05.034. URL: https://www.sciencedirect.com/science/article/pii/S0096300310005783.

[15] M. Giles et al. "Adjoint equations in CFD - Duality, boundary conditions and solution behaviour". In: *13th Computational Fluid Dynamics Conference*. DOI: 10.2514/6.1997-1850. eprint: https://arc.aiaa.org/doi/pdf/10.2514/6.1997-1850. URL: https://arc.aiaa.org/doi/abs/10.2514/6.1997-1850.

[16] Mike Giles and Niles Pierce. "An Introduction to the Adjoint Approach to Design". In: *Flow, Turbulence and Combustion* 65 (Apr. 2000). DOI: 10.1023/A:1011430410075.

[17] Snorri Gudmundsson. *General Aviation Aircraft Design*. ELSEVIER, 2022. ISBN: 978-0-12-818465-3.

[18] Max D. Gunzburger. *Perspectives in Flow Control and Optimization*. Society for Industrial and Applied Mathematics, 2002. DOI: 10.1137/1.9780898718720. eprint: https://epubs.siam.org/doi/pdf/10.1137/1.9780898718720. URL: https://epubs.siam.org/doi/abs/10.1137/1.9780898718720.

[19] Björn Gustafsson. "Quadrature Identities and the Schottky Double". In: *Acta Applicandae Mathematicae* 1 (1983), pp. 209–240. URL: https://people.kth.se/~gbjorn/schottky.pdf.

[20] Nancy Hall. *Conformal Mapping - Joukowski Transformation*. Last accessed 23 October 2023. 2021. URL: https://www.grc.nasa.gov/www/k-12/airplane/map.html.

[21] Johan Helsing and Rikard Ojala. "On the evaluation of layer potentials close to their sources". English. In: *Journal of Computational Physics* 227.5 (2008). The paper appeared electronically November 28, 2007, and subsequently in the paper issue of the journal February 20, 2008. The information about affiliations in this record was updated in December 2015. The record was previously connected to the following departments: Numerical Analysis (011015004), pp. 2899–2921. ISSN: 0021-9991. DOI: 10.1016/j.jcp.2007.11.024.

[22] Dr. Russell L. Herman. *Poisson's Equation in a Disk*. 2021. URL: http://people.uncw.edu/hermanr/pde2/Poisson_in_Disk.pdf.

[23] Antony Jameson. "Aerodynamic Design via Control Theory". In: *Journal of Scientific Computing* 3 (Dec. 1988). DOI: 10.1007/BF01061285.

[24] Stephen J. Wright Jorge Nocedal. *Numerical Optimization - Second Edition*. Springer Series in Operations Research and Financial Engineering. Springer, 2006. ISBN: 0-387-30303-0.

[25] Tara LaForce. *PE281 Boundary Element Method Course Notes*. Last accessed 23 October 2023. 2006. URL: https://web.stanford.edu/class/energy281/BoundaryElementMethod.pdf.

[26] Peter D. Lax. *Functional Analysis*. Pure and Applied Mathematics: A Wiley-Interscience Series of Texts, Monographs and Tracts. WILEY - INTERSCIENCE, 2002. ISBN: 0-471-556-04-1.

[27] Ming-Gong Lee et al. "Conservative schemes and degenerate scale problems in the null-field method for Dirichlet problems of Laplace's equation in circular domains with circular holes". In: *Engineering Analysis with Boundary Elements* 37.1 (2013), pp. 95–106. ISSN: 0955-7997. DOI: https://doi.org/10.1016/j.enganabound.2012.08.009. URL: https://www.sciencedirect.com/science/article/pii/S0955799712001762.

[28] Pritpal Matharu and Bartosz Protas. "Optimal Closures in a Simple Model for Turbulent Flows". In: *SIAM Journal on Scientific Computing* 42.1 (2020), B250–B272. DOI: 10.1137/19M1251941. eprint: https://doi.org/10.1137/19M1251941. URL: https://doi.org/10.1137/19M1251941.

[29] R. Ojala. *Towards an all-embracing elliptic solver in 2D*. PhD Thesis, Lund University, 2011.

[30] Rikard Ojala. *Boundary integral equation methods for elliptic problems*. 2013. URL: https://www.csc.kth.se/utbildning/kth/kurser/DN2255/ndiff13/bie1-1.pdf (visited on 11/02/2023).

[31] Augusto C. Ponce and Nicolas Wilmet. In: *Advanced Nonlinear Studies* 20.2 (2020), pp. 459–475. DOI: doi:10.1515/ans-2020-2078. URL: https://doi.org/10.1515/ans-2020-2078.

[32] Bartosz Protas and Pritpal Matharu. *Miscellaneous Lecture Notes on Numerical optimization of partial differential equations*. 2018. URL: https://math.mcmaster.ca/~bprotas/lecture_notes.shtml (visited on 08/03/2023).

[33] G. Steven Gipson and B.W. Yeigh. "The unit circle trap in boundary elements redux". In: *Engineering Analysis with Boundary Elements* 32.5 (2008), pp. 431–437. ISSN: 0955-7997. DOI: https://doi.org/10.1016/j.enganabound.2007.08.009. URL: https://www.sciencedirect.com/science/article/pii/S0955799707001452.

[34] Arthur Stück. "Adjoint Navier-Stokes methods for hydrodynamic shape optimisation". In: 2012. URL: https://api.semanticscholar.org/CorpusID:124687941.

[35] Lloyd N. Trefethen and J. A. C. Weideman. "The Exponentially Convergent Trapezoidal Rule". In: *SIAM Review* 56.3 (2014), pp. 385–458. ISSN: 00361445, 10957200. URL: http://www.jstor.org/stable/24248471 (visited on 08/01/2023).